https://doi.org/10.5194/egusphere-2026-1344
Preprint. Discussion started: 27 March 2026

Analysis and modeling of coastal hazards to the desalination plants in the Baltic Sea - disentangling the impacts of a coastal storm in summer 2023

Matteo Masini[(a),(b)], Agnes Karlsson[(c)], Lars Arneborg[(d)], Bengt Karlson[(d)], and Inga Koszalka[(a),(b)]

[(a)]Stockholm University, Department of Meteorology (MISU), Stockholm, Sweden
[(b)]Bolin Centre for Climate Research, Stockholm, Sweden
[(c)] Stockholm University, Department of Ecology, Environment and Plant Sciences (DEEP), Stockholm, Sweden
[(d)]Swedish Meteorological and Hydrological Institute (SMHI), Norrköping, Sweden

Correspondence: Matteo Masini (matteo.masini@misu.su.se)

Abstract. We present an analysis of coastal hazards associated with the passage of an extreme storm named Hans in the Baltic Sea in August 2023. The storm resulted in disturbance of drinking water production at the desalination plants on Gotland, the largest island of the Baltic Sea. The limited ground water resources combined with increased demand during the warm tourist season lead to recurring seasonal water stress on Gotland. Thus, drinking water production through desalination of sea water is needed to complement the municipal water supply. The storm Hans triggered extreme water and organic material transport to the intake stations of the desalination plants clogging the filters, and coinciding with cold sea temperature spells, that collectively disturbed the water treatment process. We analyze the ocean-dynamical drivers of these coastal hazards and their impacts, and present a pathway toward a tailored forecast system to the desalination plants combining available observations, operational ocean model outputs, and statistical models. The linear coastal response to southwesterly winds of storm Hans was found to be the primary driver, either directly or indirectly, of the coastal hazards impacts. The linear regression models building upon this finding show a potential for future development of forecast framework to inform the water management on Gotland, if continued reporting and observational efforts can be secured.

1 Introduction

Natural hazards are naturally occurring extreme events that have a negative effect (hazard impact) on human health, industries, and environmental services (Merz et al., 2020). Many of these natural hazards are of hydrometeorological character (storms, storm surges, flooding, and droughts), and significant knowledge gaps have been identified regarding the drivers and causal links between the local extreme events, large-scale atmospheric circulation, and

https://doi.org/10.5194/egusphere-2026-1344
Preprint. Discussion started: 27 March 2026

climate change (Merz et al., 2020; Rutgersson et al., 2022). Understanding the relation of natural hazards to regional climate change and predicting their impacts have been identified as one of the Grand Challenges in the Baltic Sea region (Meier et al., 2014, 2022). Forecasting hazard impacts includes: (1) identifying the drivers and predictors of natural hazards, (2) quantifying the hazard impacts from (typically) sparse and non-homogeneous data (historical records of disturbances in agriculture, infrastructure, human health) and (3) the development of either probabilistic methods or deterministic functions relating the hazards and their impacts (Merz et al., 2020). Forecasting of hazard impacts can be further complicated by the compound nature of hazard events, i.e., interaction and/or concurrence of several hazards (Merz et al., 2020; Rutgersson et al., 2022). This is often the case in coastal regions where hazards are caused by oceanic processes with atmospheric and biogeochemical drivers featuring time scales ranging from hours to several years. A better understanding of compound coastal hazards, their drivers, the probability of occurrence, and consequences is needed to enable prediction and development of adaptation and mitigation strategies (Contestabile and Vicinanza, 2020). Large amounts of data from operational numerical models, assimilated with observations, are provided and made publicly available through international initiatives. Bridging operational service data with documented coastal hazard impacts is valuable both from a scientific perspective (i.e., filling knowledge gaps) and from a service perspective by evaluating their relevance to user needs (Martín Míguez et al., 2026).

1.1 Water resources on Gotland, coastal hazards and their impacts

Gotland is Sweden's largest island located in the middle of the Baltic Sea (Fig. 1) with a population of about 60,000, employed in services, the food industry and the tourism sector(*https://gotland.se/region-och-politik/regionfakta-och-statistik/fakta-om-ons-naringsliv*, *J. Nilsson, pers. comm.*). Gotland's hydrological conditions, thin soil layers, impermeable rock, and drainage from agriculture, make much of the precipitation running off into the surrounding Baltic Sea resulting in limited ground water reservoirs. The island hosts seasonal residents and tourists (over 500,000 registered guest nights from May to September 2024, *https://www.regionfakta.com/gotlands-lan/*), leading to recurring water stress (the demand for water exceeds the available amount) during spring-summer. Water availability (the sum of precipitation and snowfall minus evapotranspiration) is an indicator of the availability of both surface and groundwater resources. As a consequence of climate change in the region, the decrease in water availability on Gotland for spring-summer during 2021-2050 compared to the reference period 1961-1990 was estimated to be about 20% (Johansson, 2020). The water stress is further amplified in the periods of extreme summer heat spells (heatwaves), predicted to increase in frequency and intensity in Europe and Scandinavia in response to climate change (Russo et al., 2015, Figures 3-4). Thus, Region Gotland faces a challenge to secure the future drinking water and sustainable management of water resources, seeking alternative solutions to the groundwater based supply. There are currently over 20 different water plants on Gotland, including the groundwater treatment plants, surface water plants and ones that treat water from a stone quarry, and two are desalination plants (Johansson, 2020), which are in focus of this study.

https://doi.org/10.5194/egusphere-2026-1344
Preprint. Discussion started: 27 March 2026

Desalination plants are water treatment plants that produce drinking water from sea water. Desalination is a several-step process starting with pumping of sea water by a submerged intake pump to an intake station on land, filtering of organic and inorganic material, UV-treatment for bacteria and viruses, nanofiltering (removal of sea water salt ions by pressing the sea water through a fine filter membrane) and mineralization of the purified water to the drinking water (Salinas-Rodriguez and Schippers, 2021; Yang et al., 2019). Desalination is an attractive method for drinking water production as it does not put any stress on land freshwater resources and could potentially provide an almost unlimited amount of water (Silva Pinto and Cunha Marques, 2017). Two desalinization plants have been built on Gotland since 2016 to support the municipal water supply infrastructure and reduce water stress: in Kvarnåkershamn (southwest Gotland coast) and Herrvik (eastern Gotland coast), see figure 1. Their theoretical maximum drinking water producing capacity reaches 70% of the total island's demand.

The ALGOTL project is an interdisciplinary collaboration between Stockholm University, the Swedish Meteorological and Hydrological Institute (SMHI) and Region Gotland that aims to integrate the observational and modeling expertise to develop a forecast framework for algae blooms and related hazards to support the management of water resources on Gotland, including the desalination plants, as the algae (phytoplankton) blooms were reported to have caused the disruption in the desalination process on Gotland, as in other geographical locations e.g., in the Persian Gulf (Anderson et al., 2017; Villacorte et al., 2021). The project workshops with stakeholders (The Water Management on Region Gotland) helped to identify the coastal hazards that cause negative hazard impacts to the desalination process (disturbance in operation and/or a need for extra maintenance). The negative impacts were primarily associated with the sea water intake though the intake pipes submerged close to the bottom, 6-10 m below the surface, and about 1 km from the coast. These coastal hazards and their negative impacts are summarized as follows:

1. **Hazard:** Strong water velocity (volume transport) events (called hereafter *coastal storms*), tearing off, stirring and whipping up organic material in the vicinity of the desalination plant.
   Hazard impact: Organic matter cause *clogging* of the intake pipes, and sometimes even of filter membranes on land, reducing the water intake and requiring costly manual maintenance.
   Occurrence: Year round and are associated with meteorological (wind) forcing (i.e., atmospheric storms).

2. **Hazard:** Sudden (hourly-time scale) sea temperature drops below 12^{o} C at the intake pipe during (cold spells).
   Hazard impact: Require a change in water treatment operating mode from summer to winter.
   Occurrence: Summer (June-September). Does not cause a severe disruption by itself, only if it occurs as compound hazard with coastal storms [1] adding to overall burden.

3. **Hazard:** High turbidity.
   Hazard impact: A general decrease in water quality and higher costs of filtering.
   Occurrence: Often associated with coastal storms [1] due to wind-driven mixing, and during phytoplankton blooms, frequently dominated by cyanobacteria during summer (Hajdu et al., 2007).

https://doi.org/10.5194/egusphere-2026-1344
Preprint. Discussion started: 27 March 2026

.

These coastal hazards are driven by meteorological conditions: extreme wind storms, upwelling-favorable winds, and marine heat waves, and can occur in a compound form leading to water stress during warm tourist season when the water demand increases.

1.2 Coastal hazards of storm Hans and their impacts

In summer 2023, two strong atmospheric storms were recorded by the meteorological stations on Gotland (Fig. 1). In the beginning of July, strong southwesterly (SW) winds were associated with the storm Poly that caused a havoc in western Europe (EUMETSAT: *https://user.eumetsat.int/resources/case-studies/storm-poly*). On August 6-11 2023, an extreme storm called Hans swept through the Scandinavian peninsula (*https://www.smhi.se/kunskapsbanken/meteorologi/stormar-i-sverige/20240222/norden*). Hans caused traffic disruptions, floods, mudslides and landslides in Sweden (*https://www.krisinformation.se/en/hazards-and-risks/disasters-and-incidents/2023/storm-hans*) and was deemed as one of the most destructive in Sweden of the last decade (SMHI Faktapaket: *https://www.smhi.se/kunskapsbanken/meteorologi/stormar-i-sverige/20240222/norden*). The passage of Hans was recorded on Gotland between the 8th and the 13th of August (Fig. 1, the wind speed field from atmospheric reanalysis during the peak of Hans is also shown; see sect. 2 for the description of observations and model outputs).

The SW winds associated with Poly and Hans triggered a region-scale response seen in sea state reanalysis (Fig.2). An intense upwelling along the western Baltic coast leading to a drop of the sea surface temperature (SST), which for Hans were extending over 100 km offshore (Fig.2a,d). Dropping surface temperatures hampered the ongoing cyanobacterial bloom (Fig.2b,e). Intense vertical mixing was modelled along the eastern Baltic coasts (Fig. 2c,f) where the downwelling of surface waters led to a weaker stratification.

On 8 August 2023, Region Gotland's technical personal reported that the operation of the desalination plant in Kvarnåkershamn was severely disturbed during the passage of Hans. High sea current velocities stirred up organic material (identified as red macroalgae torn from the sea bottom nearby) that filled up the intake pipes and even the internal drum filters, causing problems with water pressure and pump performance. High turbidity and high waves were also observed. The disturbance required manual filter cleaning and pipe maintenance by divers. Similar disturbance incurred at the same time at Herrvik where the one filter ('microsil') had to be replaced. The event coincided with a drop in bottom water temperature at Herrvik. Although wind speeds of Poly around Gotland were only slightly lower than Hans (97th vs 98th percentile estimated over 2010-2024; Fig. 1), Poly caused no reports of significant disturbance at the desalination plants.

https://doi.org/10.5194/egusphere-2026-1344
Preprint. Discussion started: 27 March 2026

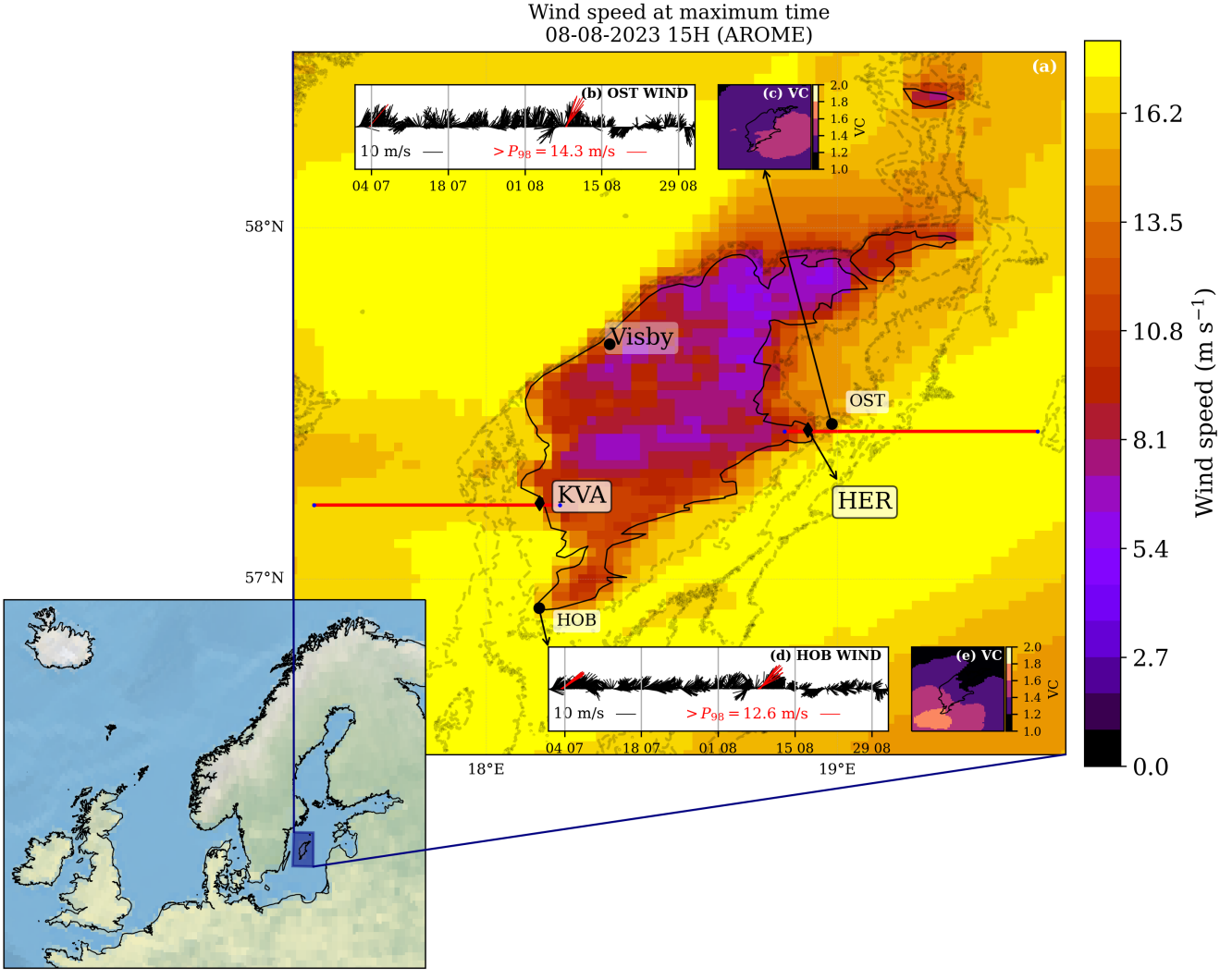

Figure 1. (a): Wind speed computed from high-resolution hourly MetCOOP/HARMONIE used as wind forcing in the ocean model (see sect. 2.2) at the time instance corresponding to the maximum wind speed in the domain during the Hans storm. Inserts show wind stick-plots at Osterngarnsholm (b, OST) and Hoburg (d, HOB) in July-August 2023 (each stick indicates the direction in which the wind is blowing toward). In (c) and (d), red sticks indicate wind speed larger than 98th percentile based on 2010-2024 period. Vector correlation between wind vectors in MetCOOP/HARMONIE at every grid point with the observations at SMHI stations are shown as inserts (c, OST) and (e, HOB). EMODNET (http://www.emodnet-bathymetry.eu/) bathymetry contours of 20, 40 and 60 m are plotted in gray, the coast is plotted in black. Location of the desalination plants are marked as HER (Herrvik) and KVA (Kvarnåkershamn). Transects used for Principal Component analysis are also shown as red lines (Section 2.3.4).

https://doi.org/10.5194/egusphere-2026-1344
Preprint. Discussion started: 27 March 2026

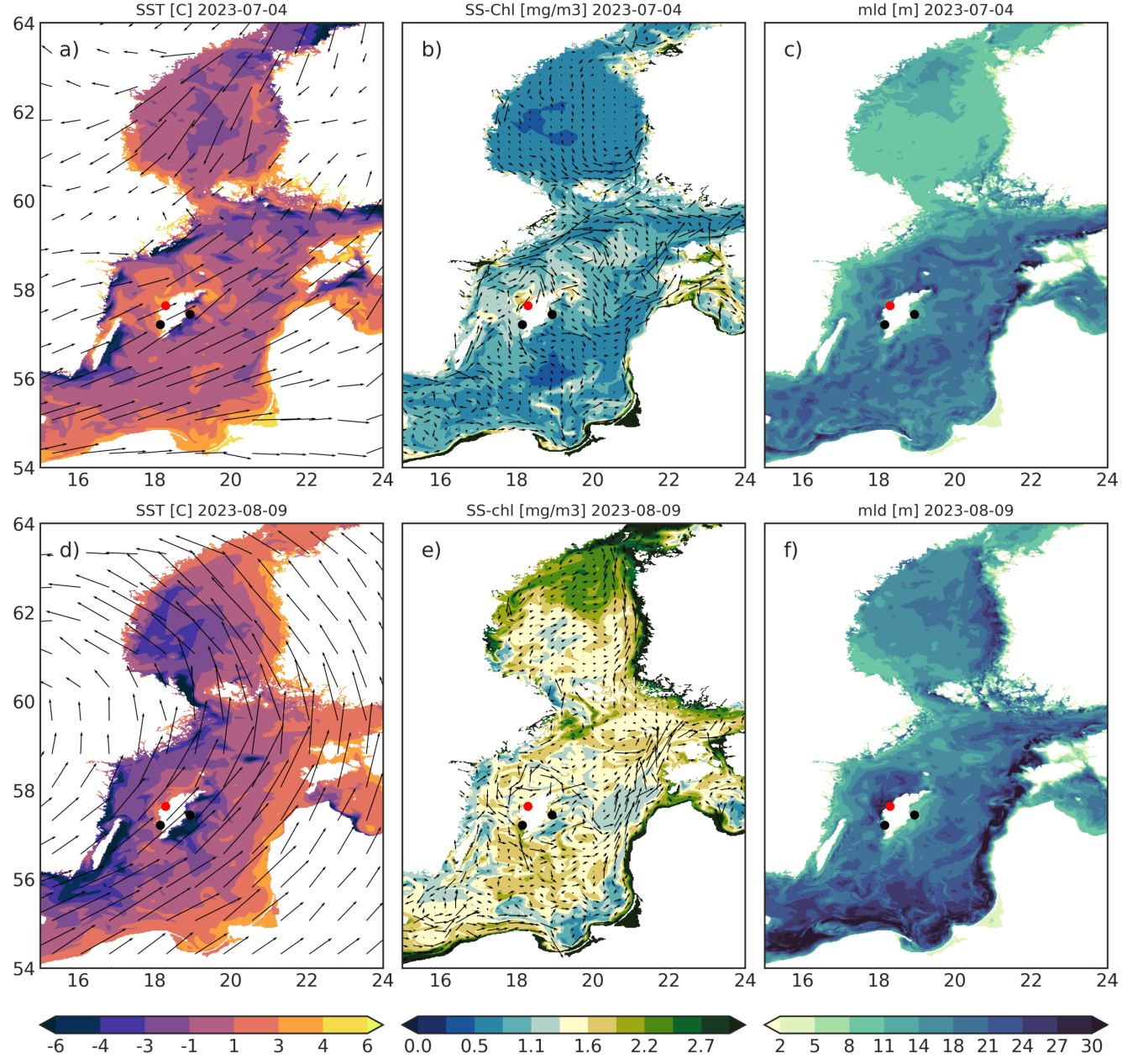

Figure 2. Ocean fields in the Baltic Sea region during Poly (2025-07-04; top), and during Hans (2025-08-09; bottom). (a,d): Sea surface temperature anomaly from the spatial average with wind vectors superimposed; (b,e): surface chlorophyll with surface ocean current vectors superimposed; (c,f): mixed layer depth (proxy for vertical mixing). Superimposed on panels (a,c) are the wind vectors preceding the shown ocean situation by 12 h, from Global Ocean Hourly Sea Surface Wind and Stress from Scatterometer and Model (*https://doi.org/10.48670/moi-00305*, accessed: 2025-10-13). Physical ocean variables: Baltic Sea Biogeochemistry Reanalysis (*https://doi.org/10.48670/moi-00013*, accessed: 2025-10-13). Chlorophyll: Baltic Sea Biogeochemistry Reanalysis (*https://doi.org/10.48670/moi-00012*, accessed: 2025-10-13). The position of the desalination plats on Gotland (see text) is marked with black circles and the town of Visby is marked with red circle.

https://doi.org/10.5194/egusphere-2026-1344
Preprint. Discussion started: 27 March 2026

1.3 The approach

The aim of this study is to analyze the coastal hazards associated with the passage of Hans storm and their negative impacts on the desalination production drinking water on Gotland, in view of developing an observational, analysis and forecast framework to secure future water resources on Gotland.

Our approach can be summarized as follows:

Reported impact $\Longrightarrow$ Analysis $\Longrightarrow$ Identify the drivers $\Longrightarrow$ Develop physics-based impact forecast

We build upon the **reports** about coastal hazards and their negative impacts on the desalination plants on Gotland associated with the passage of Hans storm in August 2023.

For the **analysis**, we use the available observations and model outputs to identify the drivers of the hazards. As oceanographic observations at sea close to the desalination plants are missing, we use available sea state forecast and reanalysis products based on the output from an operational ocean model (sect. 2.2). Water temperature and salinity observations from the intake station at Kvarnåkershamn in summer 2023 are available. These observations are not fully representative of sea water conditions outside the station, but are helpful in making the connection between the model outputs and the impacts recorded in the desalination process. We also use wind observations (sect. 2.1).

We have analyzed different model **variables** and distilled these as proxies of coastal hazards [1-2] (sect. 1.1):

i) the horizontal sea water velocity, in particular the zonal (u) components as a proxy for cross-shore velocity. These, multiplied by cross-sectional model grid area, yield volume transports (U) that serve as proxy for material transport to the intake pipe that cause clogging. The negative impact associated with Hans corresponded to U exceeding 3.5 standard deviation over summer 2023 at both stations (sect. 3.1.2).

ii) the sea bottom temperature (T_b), a proxy for the intake water temperature at the pipes leaning against the bottom. The condition $T_b < 12^\circ$ C (or equivalently $T_b/12^\circ C \leq 1$) during the summer was reported as the negative impact prompting the change to winter operation mode.

Other ocean model variables are used complementarily to describe the oceanographic context.

To **identify the drivers**, we isolate the conditions associated with storms Hans (negative impacts at the desalination plants) compared to Poly (no negative impacts).

Finally, we test the performance of linear regression-based **hazard impact forecast models** informed by theory and analysis results for the variables mentioned above. Models of higher complexity and alternative approaches based on data-driven methods, as well as turbidity (coastal hazard [3], sect. 1.1), will be analyzed elsewhere.

1.4 Candidate oceanic drivers of coastal hazards

We expect that the following oceanic processes could contribute to the coastal impacts at the desalination plants associated with the passage of Hans:

https://doi.org/10.5194/egusphere-2026-1344
Preprint. Discussion started: 27 March 2026

1) **Wind-driven coastal upwelling and downwelling** The Baltic Sea is characterized by transient (changing over a scale of a few days) and predominantly along-shore (with respect to the Gotland's geometry) winds, with south-westerly (SW) winds blowing about 30-40% of the time (Soomere and Keevallik, 2001; Masini et al., 2025); SW winds were prevailing over the month of July 2023 and pronounced during both storms, Poly and Hans (Fig. 1). The coastal ocean response to SW winds develops over the inertial period (about 14 h in the Baltic Sea) and consist of a horizontal (Ekman) transport of surface waters away (towards) the eastern (western) Gotland coast generating divergence in the currents and coastal upwelling (convergence in the currents and coastal downwelling), and development of coastal jets (ocean currents in the direction of the wind and with velocity increasing in time) intensified at about 20 km from the coast (Masini et al., 2025). The Baltic Sea features a permanent halocline at about 60 m depth and a summer thermocline at 15-20 m depth (Leppäranta and Myrberg, 2009) and the surface Ekman layer depth is comparable to that (Masini et al., 2025). Assuming a two-dimensional and steady state, most of the onshore (offshore) bottom flow associated with the upwelling (downwelling) would be confined in the bottom boundary layer at the SW and SE coasts of Gotland which feature gentle slopes and weak stratification (Lentz and Chapman, 2004; Masini et al., 2025). During upwelling events in the summer, the thermocline shoals and sometimes outcrops leading to baroclinic instability as early as four days from the onset of the moderate wind events, resulting in meandering and generation of eddies that are interacting with complex topography (Zhurbas et al., 2006; Masini et al., 2025).

2) **Inner shelf** In the presence of shallow bathymetry and under sufficient alongshore wind strength and duration, the coastal jets over the sloping bottom might undergo a separation from the coast and an "inner shelf" circulation might develop between the coast and the coastal jet, associated with intense vertical mixing (stronger for downwelling due to convergence of surface waters towards the coast and lower stratification, (Austin and Lentz, 2002)). The inner shelf circulation might lead the accumulation of algae and other buoyant material (downwelling) or re-suspended material (upwelling) at the coast (Austin and Lentz, 2002; Masini et al., 2025).

3) **Coastal trapped waves** Alongshore variations in coastline and bathymetry or spatial variations in winds can excite sea level and pycnocline disturbances propagating as coastal trapped waves (CTWs); and the vertical thermocline displacements associated with these waves can cause the bottom temperature variability (Walin, 1972a, b; Fennel and Seifert, 1995). CTWs have been suggested as an explanation for why the upwelling appears frequently only on the southeastern coast of Gotland during SW winds: the downwelling signal excited at the northern Gotland propagates with CTWs southward along the eastern coast of Gotland (where Herrvik is located), reducing the upwelling signal there. A slower phase speed due to shallower waters and coastal curvatures hinders export of upwelling further around the southern tip resulting in generation of large upwelling cell at the Gotland's southern east coast (Fennel et al., 2010). This frequent upwelling on the southeastern coast of Gotland and the southern upwelling cell has been conspicuous features seen in remote

https://doi.org/10.5194/egusphere-2026-1344
Preprint. Discussion started: 27 March 2026

sensing images (Lehmann et al., 2012). CTWs have also been observed on the northwestern Gotland's coast side (Pizarro and Shaffer, 1998).

4) **Vertical mixing** associated with strong winds (Kullenberg, 1981), and pronounced at the coast during downwelling (see [2] and references herein) and inner shelf circulation (see [3] and refrences herein) will homogenize the water column temperature, algae and other material close to the coast where the desalination plants are located.

5) **Organic material accumulations due to phytoplankton blooms**, specifically cyanobacteria (toxin-producing *Nodularia spumigena* and non-toxic *Aphanizomenon spp.*) dominating in the Baltic Sea during the summer (Kahru et al., 2007; Karlson et al., 2021; Ledesma et al., 2022). Phytoplankton blooms, that develop primarily close to the surface, will be redistributed in the water column by vertical mixing and strong ocean currents during storms. Coastal upwelling and downwelling will have further consequences for phytoplankton. Upwelling brings into the surface the cold bottom waters (limiting the growth of cyanobacteria dominating during the summer as well as nutrients (promoting in general the growth of all phytoplankton types) and the convergence associated with downwelling and inner shelf (see [1] and [2]) will cause accumulation of at the coast (Lips and Lips, 2008; Lass et al., 2010; Zhurbas et al., 2008; Dabuleviciene et al., 2020). Although modern desalination systems are generally effective at removing phytoplankton and cyanobacterial toxins from seawater, the increased total suspended solids and organic content resulting from phytoplankton biomass in sea water (extracellular polysaccharides and glycoproteins giving the organic accumulations a gelatinous appearance and characterized by high stickiness and adhesion tendency) contributes to clogging/fouling of pretreatment system and the increased membrane fouling (Caron et al., 2010; Villacorte et al., 2015; Anderson et al., 2017; Villacorte et al., 2021).

6) **Macroalgae intake and clogging.** Macroalgae can be detached from the seafloor due to high bottom shear stress caused by currents or strong wave action. Once floating they can be transported to the intake pipes contributing to the clogging of filters. Macroalgae extent and potential re-suspended material from them are not easily quantified using satellites in the dark waters of the Baltic (Vahtmäe et al., 2021). Because the algae clogging has been reported as a disturbance occurring year round during strong storm events, we will assume that the volume (velocity) transport can be used as proxy for this hazard.

.

Since coastal processes [1-3] can be directly diagnosed from the simulated ocean state variables and linked to the reported impacts, in the following analyses we focus on these, while we assume processes [4-6] will be adding up to the negative impacts [1-3].

https://doi.org/10.5194/egusphere-2026-1344
Preprint. Discussion started: 27 March 2026

2 Material and methods

2.1 Observations

To relate the storm impact reports from the desalination plants to meteorological conditions and to evaluate the wind forcing of the operational ocean model, we use the available closest wind observations. Hourly wind speed and direction were downloaded from the SMHI's database (https://www.smhi.se/data/hitta-data-for-en-plats/ladda-ner-vaderobservationer/wind/) at Hoburg (HOB, ID = 68560) (southern tip of Gotland) and Österngarnsholm A (OST, ID = 78280), 4.5 km offshore from Herrvik (Figure 1). Observations were accessed on 12-04-2024 and considered the period 1 July-1 September 2023. Only quality-marked observations were used (99.93% observations in this period).

In-situ temperature (ITS-90) and conductivity measurements were conducted by SMHI inside the intake station of the desalination plant in Kvarnåkershamn using Sea-Bird Electronics Inc. SBE 37-SM at sampling rate of 600 seconds in the period 29 June-13 September 2023. The raw data were processed using SeatermV2 2.8.0.119 software. These data are used to describe the temperature and salinity conditions at the intake and related to the ocean model results (sect. 3.1.3), but they cannot be used directly to represent the oceanographic conditions in the sea outside the intake station or to evaluate the performance of the ocean model.

2.2 Sea state forecast and reanalysis model output

For 2023, we used the Baltic Sea Physics Analysis and Forecast product (https://doi.org/10.48670/moi-00010) publicly available at the Copernicus Marine Services (CMEMS) website. This operational sea state product is based on NEMOv4.2.1 ocean model (Kärnä et al., 2021) at the horizontal resolution of 1 nm (ca. 1,852 km) and 56 vertical depth levels (1 m resolution near the surface and about 24 m in the deepest layers). The atmospheric forcing consist of the control member of the AROME-MetCoop system (Müller et al., 2017) at the horizontal resolution of 2.5 km and hourly output for the first 66 hours, and ECMWF (11 km horizontal, varying temporal resolution, see (Bauer et al., 2013) for details) deterministic forecast thereafter. The surface velocity includes Stokes drift from the Baltic Sea Wave forecast product (https://doi.org/10.48670/moi-00011). Satellite SST, sea ice concentrations and in-situ T and S profiles are assimilated into the model's analysis field. This data set is called F2023. We also use data for the following year (F2024) in order to validate the linear regression model.

We also use the chlorophyll from Baltic Sea Biogeochemistry Analysis and Forecast (https://doi.org/10.48670/moi-00009) and reanalysis (https://doi.org/10.48670/moi-00012). These products employ the biogeochemical model ERGOM (Neumann et al., 2022), which one way coupled to the aforementioned coupled to the physics' forecast and reanalysis models mentioned above as a proxy for phytoplankton bloom intensity in a general overview of regional response (Fig. 2, sect. 3.1.1). This product is no validated close to the coast for we do not use it for detailed analyses close to the desalination plants.

https://doi.org/10.5194/egusphere-2026-1344
Preprint. Discussion started: 27 March 2026

2.3 Analysis methods

2.3.1 Vector correlation

Observations from both Hoburg and Östergarnsholm are assimilated in ocean model wind forcing, the AROME-MetCoop system (Müller et al., 2017). The correspondence between the wind observations and the wind forcing can be evaluated through the vector correlation ρ_v (Crosby et al., 1993):

$$\rho_v^2 = \mathrm{Tr}\left[(\Sigma_{11})^{-1}\Sigma_{12}(\Sigma_{22})^{-1}\Sigma_{21}\right] \tag{1}$$

where:

$$\Sigma = \begin{pmatrix} \mathrm{Var}(u^w_{\mathrm{obs}}) & \mathrm{Cov}(u^w_{\mathrm{obs}}, v^w_{\mathrm{obs}}) & \mathrm{Cov}(u^w_{\mathrm{obs}}, u^w_{\mathrm{AROME}}) & \mathrm{Cov}(u^w_{\mathrm{obs}}, v^w_{\mathrm{AROME}}) \\ \mathrm{Cov}(v^w_{\mathrm{obs}}, u^w_{\mathrm{obs}}) & \mathrm{Var}(v^w_{\mathrm{obs}}) & \mathrm{Cov}(v^w_{\mathrm{obs}}, u^w_{\mathrm{AROME}}) & \mathrm{Cov}(v^w_{\mathrm{obs}}, v^w_{\mathrm{AROME}}) \\ \mathrm{Cov}(u^w_{\mathrm{AROME}}, u^w_{\mathrm{obs}}) & \mathrm{Cov}(u^w_{\mathrm{AROME}}, v^w_{\mathrm{obs}}) & \mathrm{Var}(u^w_{\mathrm{AROME}}) & \mathrm{Cov}(u^w_{\mathrm{AROME}}, v^w_{\mathrm{AROME}}) \\ \mathrm{Cov}(v^w_{\mathrm{AROME}}, u^w_{\mathrm{obs}}) & \mathrm{Cov}(v^w_{\mathrm{AROME}}, v^w_{\mathrm{obs}}) & \mathrm{Cov}(v^w_{\mathrm{AROME}}, u^w_{\mathrm{AROME}}) & \mathrm{Var}(v^w_{\mathrm{AROME}}) \end{pmatrix} = \begin{pmatrix} \Sigma_{11} & \Sigma_{12} \\ \Sigma_{21} & \Sigma_{22} \end{pmatrix} \tag{2}$$

where $\boldsymbol{u^w}_{(obs)} = (u^w_{(obs)}, v^w_{(obs)}))$ are observed wind vector time series at Hoburg ($\boldsymbol{u_{obs=HOB}}$) or Österngarnsholm ($\boldsymbol{u_{obs=OST}}$), and $\boldsymbol{u^w}_{\mathrm{AROME}} = (u^w_{\mathrm{AROME}}, v^w_{\mathrm{AROME}})$ are AROME wind vector time series at every ocean model grid point. The vector correlation quantifies how much two time series of vectors are inter-dependent. In other words, the perfect vector correlation ($\rho_v = 2$), between one time series of vectors indicates that either 1) the two series are identical, or 2) one series can be obtained from the other by rotation of a constant angle and/or multiplication of the magnitude by a constant value. Figure 1 shows the vector correlation between the observed wind at Östergansholm (panel c) and Hoburg (panel e) and the AROME wind forcing around Gotland. The correlation varies between 1.2 and 1.6 (moderately correlated) in the proximity of the desalination plants. The vector correlation between the SMHI wind stations and their nearest AROME grid points is 1.65 for Hoburg (Fig. 1d) and 1.57 for Östergarnsholm (Fig. 1b). These values can be interpreted as comparable to the Pearson linear correlation coefficient of 0.82 and 0.79, respectively.

2.3.2 Correlation maps

To quantify the spatial structure of the sea bottom temperature (T_b) signal (sect. 1.3), we compute linear correlation between T_b series at the model grid point closest to either desalination plant and every model grid point around Gotland in the area shallower than 60 m. The Pearson correlation coefficient was computed using Python package

https://doi.org/10.5194/egusphere-2026-1344
Preprint. Discussion started: 27 March 2026

scipy.stats.pearsonr. Only points with significant correlation at the 95% confidence level are considered (using two-sided t-test under the null hypothesis that the data is uncorrelated).

2.3.3 Hovmöller diagrams

Time-distance or Hovmöller diagrams are used to quantify directional propagation of coherent signals, for example coastal trapped waves (Persson, 2017; Fennel et al., 2010). We use time-distance diagrams here to assess the propagation of bottom temperature (T_b) signal around Gotland at selected iso-baths as well as the time-depth diagrams to assess the passage of cold sea water temperature anomalies at selected model grid points.

2.3.4 Principal Component Analysis

The dominant modes of spatiotemporal variability of the velocity (transport) close to the desalination plants was assessed by the Principal Component (PC) time series and Empirical Orthogonal Functions (EOFs) of the hourly horizontal zonal (proxy offshore) and meridional (proxy along-shore) velocity (F2023) at the zonal transects extending 40 km offshore (Figure 1). We perform the analysis for the two velocity components separately because according to the linear theory we would expect different responses to the wind forcing: for coastal upwelling and downwelling, the across-shore Ekman transport sets in within an inertial period and is independent of time thereafter, while the along-shore coastal jet velocity increases with time (Masini et al., 2025); on the other hand, the CTWs should imprint primarily on the along-shore velocity component. Choosing the transect orientation "perpendicular to the coast" was non-trivial because of the complex bathymetry of the ocean model (that is also resolved only at the 1 nm resolution by the ocean model). We tried different transect orientations which gave slight, but rather inconclusive differences in the computed diagnostics, and finally selected the zonal orientation for simplicity.

The time series from each model point along the transect were standardized by removing the mean and dividing by the standard deviation, and filtered using a Butterworth filter with a 14-hour window and order 6 to suppress the inertial and higher frequency variability. This filter has a sharp frequency response and minimal distortion of low frequency variability (Roy et al., 1997; Koszalka et al., 2009). Covariance matrices, eigenvectors and eigenvalues were computed using numpy.linalg.eig in Python, which is implemented using LAPACK routines. The eigenvalues λ_k are sorted and $\lambda_k / \sum_j \lambda_j$ quantify fractional contribution of the corresponding eigenvector (mode of variability) k to the total variance of the field (Von Storch and Zwiers, 1999).

The PC/EOF results for water temperature and density are not included because they were affected by the progressive summer warming and concurrent vertical thermocline deepening, and hence inconclusive.

2.3.5 Linear regression

Material (volume) transport

https://doi.org/10.5194/egusphere-2026-1344
Preprint. Discussion started: 27 March 2026

The material (volume) transport is estimated from the depth-integrated ocean model velocity field:

$$(U,V) = \frac{1}{H}\left(\int_{-H(x,z)}^{0} u dz', \int_{-H(x,z)}^{0} v dz'\right) \tag{3}$$

with $H(x,y)$ as the local sea depth. For the zonal transport (proxy cross-shore), the construction of the regression model is guided by the linear coastal theory. For constant vertical viscosity, the zonal transport response to the applied wind stress develops within the inertial period (14 hr) and after that is proportional to the wind stress (Csanady, 1982a). We therefore construct a linear model with the wind stress as predictor:

$$\hat{U} = A_0 + A_1 \tau_y^{\mathrm{rot}=15^\circ} + \epsilon. \tag{4}$$

where $\tau_y^{\theta_r=15^\circ} = c_d \rho_a v_y^{\theta_r=15^\circ} \mid v_y^{\theta_r=15^\circ} \mid$ is the wind stress at Hoburg (HOB) projected onto a direction $\theta_r = 15^\circ$ clockwise from the North, computed by assuming the drag coefficient constant $c_d = 1.5 \cdot 10^3$ and air density is $\rho_{air} = 1.223$ kg m^{-3}. A_0, A_1 are the regression coefficients, and ϵ is the residual that we estimated with the Root Square Mean Error. The linear model has also been tested for different wind projection orientations, see Figure A4 in the Appendix.

Bottom temperature

According to the linear theory for wind-driven coastal upwelling and downwelling, displacement of free surface and density (temperature, salinity) interfaces near-shore is linear with the along-shore wind impulse (Csanady, 1982a) and this has been shown to hold during the first few days in idealized numerical simulations of the Western Gotland Basin (Masini et al., 2025). Because waters colder than 12 ° C are found below the summer thermocline, we investigate whether wind impulse can be used to predict the drops in bottom temperature below 12° C at the desalination plants by employing a linear regression model:

$$\hat{T}_{b12} = \alpha_0 + \alpha_1 I_{as} + \epsilon, \tag{5}$$

where predicted variable $\hat{T}_{b12}$ is the bottom temperature (scaled by a factor of 12) at the model grid points close to the desalination plants, α_0 and α_1 are respectively, an intercept constant and the linear regression coefficient, ϵ is the residual (root-mean-square-error, RMSE) difference between the data T_{b12} and the predicted $\hat{T}_{b12}$ and I_{as} is the wind impulse (predictor) defined as:

$$I_{as}(t) = \int_{t-\Delta t}^{t} \tau_y^{\theta \mathrm{r}=15^\circ}(t')\, dt' \tag{6}$$

The wind impulse at a given time instance is thus the wind stress integrated over the previous $\Delta t = 5$ days. The five day period is a typical duration of SW winds events in the region (Masini et al., 2025). Regression model has

https://doi.org/10.5194/egusphere-2026-1344
Preprint. Discussion started: 27 March 2026

been trained on F2023 (sample of 1464 points, corresponding to 61 days, from 1th of July till 31th of August) in every grid point around Gotland. We validate the model using ocean model data for the following summer (F2024). We performed the analysis for various rotation angles and integration time periods, and the chosen parameters were best in terms of determination coefficient R2 at the locations of both desalination plants and found that the results are insensitive to the wind rotation over a range of angles [0-25°] (Fig. A4). We choose to winds at HOB station instead of OST (Fig.1) because of a slightly larger R^2 with about the same number of predicted cold spells in HER (see sect. 3.2.2). This is presumably due to the fact that winds at HOB represent better the effect of Gotland's orography while the OST station os located further off-shore.

3 Results

3.1 Identifying drivers of the coastal hazard impacts

We begin with presenting oceanographic conditions around Gotland during the storms Poly and Hans using the ocean model output. Subsequently, we analyze the selected hazard proxy variables (sect. 1.3): the water volume transport and the bottom temperature. In the following, we will refer to the desalination plant in Kvarnåkershamn as KVA, and the one at Herrvik as HER.

3.1.1 Regional ocean response to storms

Both Poly and Hans, were associated with strong SW winds, whereby the regional-scale linear ocean response is coastal upwelling of cold waters on the eastern Swedish coast and the eastern Gotland coast and downwelling on the western Gotland coast (sect. 1.4). This response is to some extent seen in ocean model SST (Fig. 2a,d) and surface velocity (Fig. 2b,e), but the ocean circulation is more complex. While a coastal upwelling jet develops along the southeast Gotland's coast (where HER is located), the ocean response along the southwest Gotland's coast (where KVA is located) is dominated by the eastward Ekman transport due to the extreme upwelling at the Swedish coast that fills the surface Western Gotland Basin (the channel-like basin bounded by the Swedish coast and Gotland) with cold water, forcing a southward surface export flow between Gotland and Öland (offshore of KVA). Interaction of the flow with topography and/or baroclinic instability causes flows in the Western Gotland Basin to meander and recirculate north of Gotland. The ocean response around Gotland is in general stronger for Hans (Fig. 2d-f) than Poly (Fig. 2a-c). Surface chlorophyll decreases in areas of upwelled cold and salty water as well as in areas of high wind-driven vertical mixing, reflecting the inhibiting effects on growth of the cyanobacteria dominating summer phytoplankton bloom accumulations (sect. 1.4). The wind-driven mixing is reflected also in the model mixed layer depth (Fig. 2c,f) being shallower (more stratified, less mixing) in upwelling regions, and deeper (extending down to 30 m or entire water column) where the warmer, fresher,and lighter surface waters are downwelled.

https://doi.org/10.5194/egusphere-2026-1344
Preprint. Discussion started: 27 March 2026

3.1.2 Volume (material) transport

The zonal (proxy cross-shore) and vertically averaged ocean velocity serves as a proxy for the material transport to the intake pipes causing clogging of filters (Sect. 1.3), while the meridional (proxy along-shore) velocity is used as an auxiliary variable to investigate the dynamical setting.

Figure 3a shows time series of alongshore wind stress at HOB and panels (b) and (c) show time series of the vertically averaged cross-shore velocity (transport) U at the model grid points closest to, respectively, HER and KVA. These time series show a response to the increased wind stress during both storms, Poly and Hans, and the stronger response to Hans is linked to the extreme wind stress (nearly twice that for Poly). Note also transport fluctuations due to daily variation in the wind stress seen in panel a (the sea breeze, see sect. 1.4) are superimposed on the signal due to storms.

For HER, we note that (i) the cross-shore transport response is clearer at the points F-P (green-blue) about 2 km southward off HER where the flow direction is in agreement with the linear coastal upwelling response (sect 1.4; positive offshore flow in the surface layer, to the right of the SW winds); (ii) the flow at the closest points A-B (yellow) is very weak; (iii) the points C and D (brown, north of HER) show oppositely-signed (negative) flow (towards the coast). These results, and the distribution of U in panel (c) depict a recirculation of the upwelling coastal jet around the cape where HER is located.

The cross-shore transport close to KVA shows also a response to Poly and much stronger response to Hans, but is negative at all model points close to KVA (i.e., opposite to the Ekman transport due to SW winds, sect. 1.4).

The reverse signs of the zonal circulations are related to the local circulation patterns. Figure 3d-i shows the vertically averaged current speed and current vectors around the desalination plants during Poly (f-g) and Hans (h-i). An upwelling jet at the southeast coast of Gotland is conspicuous, and it turns north- and onshore after passing the cape where HER is located. At KVA, the southward export from the Western Gotland Basin (Fig. 2b and e) encounters a shoaling in the topography and the southern tip of Gotland (Fig. 1; isobaths between KVA and HOB) leading to a cyclonic (on-shore) recirculation close to KVA. The shallow, bay-like area offshore KVA shows daily-variations due to sea breeze and other local inner-shelf variability (sect. 1.4). Note that on both sides of Gotland, the coastal circulation is up to twice as strong for Hans as for Poly.

Figure 4 shows spatial and temporal patterns of the first Principal Component (EOF-1 and PC-1, respectively) of the zonal (proxy cross-shore, u) and meridional (proxy along-shore, v) velocity along the transects anchored at the desalination plants (shown in Figure 1). Note that the positive/negative sign of the flow relates to the phase of the oscillating flow anomaly from the time-space mean. The amount of explained variance for u is larger for the transect at HER (40.52 %) than KVA (28.04 %) suggesting that the flows at the latter site are more variable. The amount of explained variance for v is comparable at KVA and HER, about 40%.

The EOF/PC generalizes the results mentioned above: A two-layer circulation is evident at both sections, with a surface layer about 20 m thick. At KVA (Fig. 4a and c), there is a surface recirculation developing about 10 km

https://doi.org/10.5194/egusphere-2026-1344
Preprint. Discussion started: 27 March 2026

offshore due to the increased southward export flow between Öland and Gotland in response to Poly and Hans (see above). At HER (Fig. 4b and d), the flows are consistent with the expected response to wind, positive during SW winds and delayed by 14-16 hours with respect to the onset of the strong wind events. Note that v at HER, albeit consistent with a coastal jet, appears "trapped" at 20-30 m isobath, which could be a signature of CTWs (driver [3] in sect. 1.4).

Note that the PC-1 time series of v are in general hard to interpret because: i) the coastal jet speed at HER and the export flow and recirculation at KVA are the response to the wind forcing driving upwelling at southeast Gotland (directly for HER) and the Swedish coast (indirectly for KVA), ii) the CTWs will be superimposed and conflated in the meridional (proxy along-shore) velocity signal. The responses of Poly and Hans are thus less discernible in v compared to u. This confirms the notion that zonal (proxy cross-shore) transport U is a more apt proxy variable for the coastal transport due to extreme wind events in the vicinity of the desalination plants.

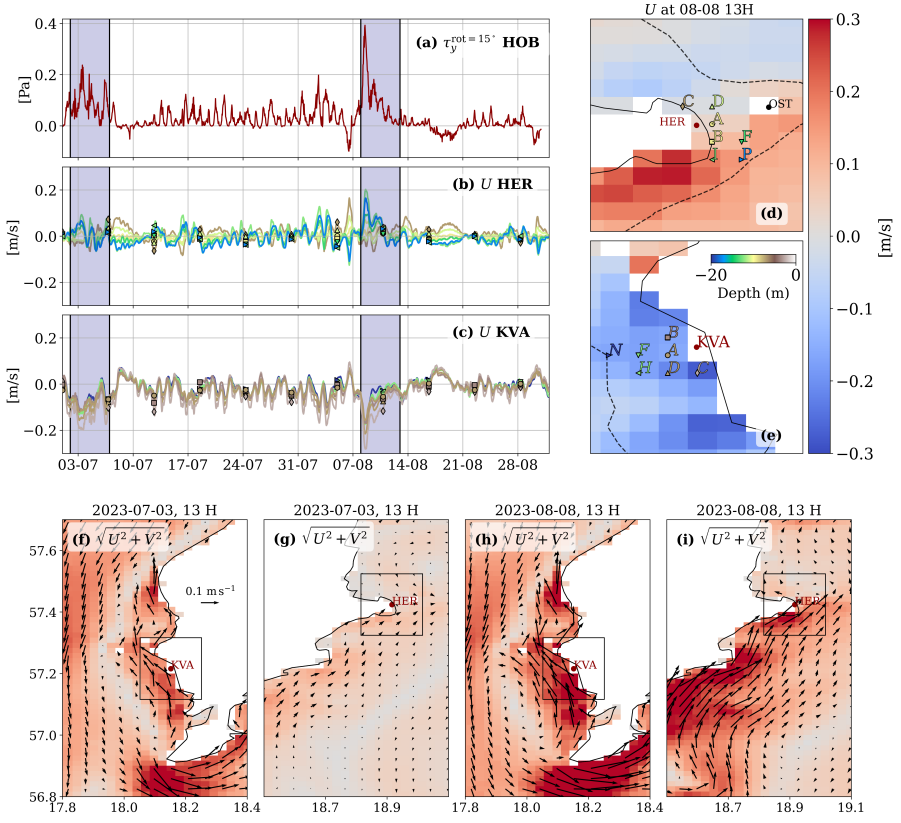

Figure 3. (a) Time series of along-shore wind stress at Hoburg (HOB). (b) Time series of cross-shore (zonal) velocities at closest points to Herrvik (HER). (c) Same for Kvarnåkershmamn (KVA). The grid points are named with capital letters according to the distance from the coast and color-coded. The position of the points and the color-code is shown on the panels (d) and (e) to the right, superimposed on the horizontal distribution of vertically-averaged zonal velocity U during storm Hans. The bottom row shows depth-averaged ocean current vectors close to KVA and HER, respectively, superimposed on the depth-averaged velocity speed for storms Poly (g-f) and Hans (h-i).

https://doi.org/10.5194/egusphere-2026-1344
Preprint. Discussion started: 27 March 2026

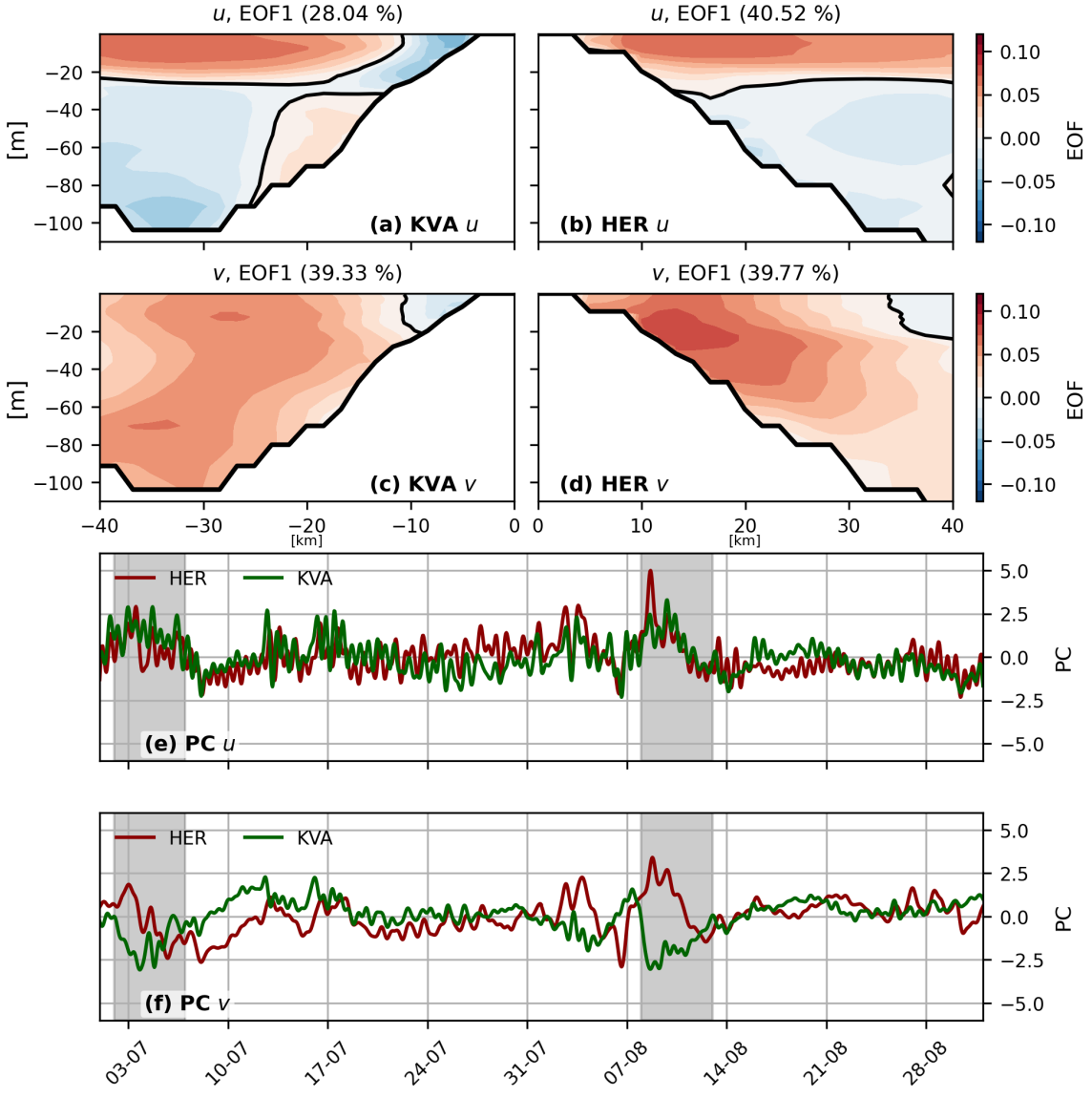

Figure 4. First empirical orthogonal functions (EOFs) of zonal (proxy cross-shore) velocities for Kvarnåkershmamn (KVA, a) and Herrvik (HER, b) along the sections shown in figure 1; (c-d) same as (a-b) but for the meridional (proxy along-shore) velocity. (e) The corresponding Principal Component time series (red for HER, green for KVA). The fraction of explained variance is given in the figure header.

https://doi.org/10.5194/egusphere-2026-1344
Preprint. Discussion started: 27 March 2026

3.1.3 Bottom temperature

Figure 5a-c shows time series of wind impulse (Eq. 6) at HOB and time series of T_b at the model grid points closest to HER and KVA. The points locations are marked in panels (d) and (e), superimposed on T_b fields on 12 August (in the middle of the Hans storm). The distance between the model grid points and the desalination plants varies between 800 and 2500 m but their relevance depends also on the local bathymetry and the model resolution. The Hovmöller (time-depth) temperature diagrams at the model grid points are shown in Appendix (Fig. A2).

At HER (panels b and d), the hazard impact condition ($T_b \leq 12^\circ$ C) is satisfied at all close grid points during both Poly and Hans and the response to the SW winds is in agreement with the linear coastal upwelling theory (sect. 1.4): the bottom temperature drop begins at the offshore points where it is most pronounced, and progresses onshore during the storms as the wind impulse increases. Note also a weaker upwelling event ($T_b \leq 12^\circ$ C preceding Hans on 5-6 August is evident in wind impulse and T_b at the deepest offshore points. The Hovmöller diagrams (Fig. A2) show that the cold bottom temperature signal in the model grid points around HER is not homogenized in the water column so the vertical mixing represented in the operational ocean model (sect. 1.4) is not so pronounced here.

At ocean model grid points close to KVA (panels c and e), the variability in T_b is generally weak for the whole period (16 $\pm 1^\circ$C). There is only one instance of upwelling-like response to the NE wind event during 17-21 August when T_b drops below 12° C at the deeper grid points (F,H). The Hovmöller (time-depth) temperature diagrams show however that the temperature is homogenized in the entire water column by mixing (sect. 1.4) during Hans storm in the model points around KVA (Fig. A2). Note that the measured temperature in the intake station (blue line) agrees very well with T_b at the close model grid points. The measured values lie between the modeled T_b at the closest points A-D and these at points F, H (further offshore), and are about one day lagged to the latter. Point F and H show the highest correlation with the observation among the grid points, respectively 0.70 and 0.69 (see Table 2). The salinity time series from the intake station at KVA (Appendix Fig. A3) show similar pattern as temperature, with low variability in July and upwelling-like response to the NE wind event during 17-21 August.

The T_b variability in the offshore point N (blue line), close to the thermocline depth of 20 m and to the 20 m isobath, is different than in the shallower points (and the intake observations): it is a few degrees colder and more complex and linked to the southwards export flow between Öland and Gotland and/or propagation of CTWs (sect. 3.1.1).

To put the results from the time series at points into regional perspective, we analyze spatial patterns of T_b around Gotland. Figure 6a shows the difference in T_b between 13th and 8th August (the duration of Hans), and panels b-c show maps of linear correlation between T_b time series at the model grid points A that are closest to HER and KVA (Fig. 5d-e), respectively, with other grid points around Gotland. The response to the wind is coherent on the eastern coast (around HER) at areas shallower than 20 meters (correlation ≥ 0.75) where T_b decreases (increases) during upwelling (downwelling). The more complex response on the south-western coast (around KVA) is also seen: a weak response to wind is coherent at areas shallower than 20 meters (correlation ≥ 0.75, Fig.6b), and a decrease in T_b along the 20 m-isobath (Fig.6a) is anti-correlated with the signal on the Gotland's eastern coast (see Fig.6c). The

https://doi.org/10.5194/egusphere-2026-1344
Preprint. Discussion started: 27 March 2026

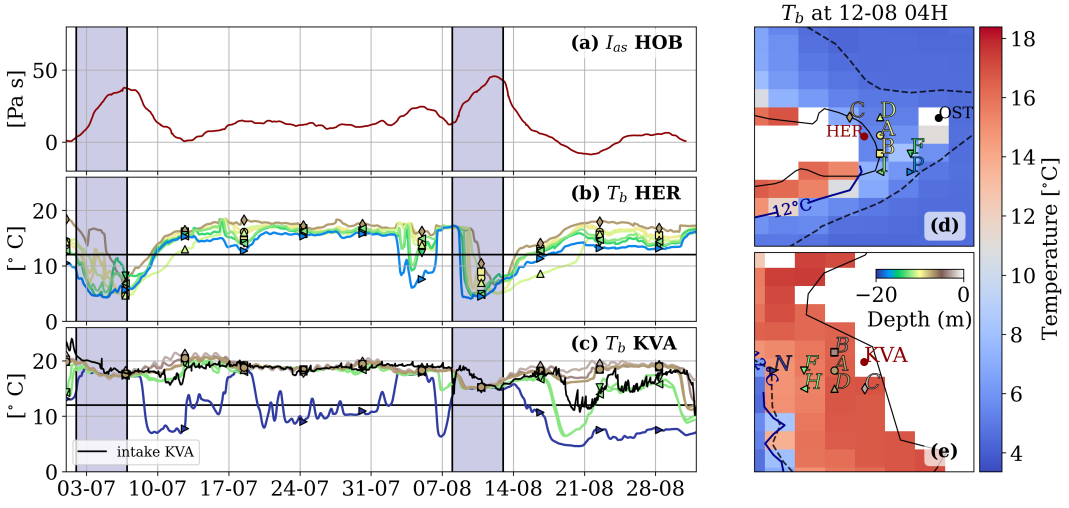

Figure 5. (a) Time series of wind impulse I_{as} (Eq.6) at HOB. (b-c) Time series of bottom temperature T_b at grid points whose location is indicated with capital letters in panels d-e. The available temperature measurement at the intake station at KVA is shown as the solid black line in panel c. Each grid point is indicated by a marker, while the color indicates the sea bottom depth (color code on panels d-e). (d-e) Bottom temperature field close to HER and KVA on 12-08-2023 (during the passage of Hans). Locations of the desalination plants (HER and KVA) are marked in red. The 20 m-isobath is shown with dashed black line and the isotherm of 12 ° C is shown with solid black line.

response to the wind is coherent on the eastern coast (around HER) at areas shallower than 20 meters (correlation ≥ 0.75) where T_b decreases (increases) during upwelling (downwelling).

A possible propagation of temperature signal from the southern tip to the western coast by CTWs (sect. 1.1 cannot be resolved in linear correlation maps. In order to investigate the signal propagation, we show Hovmöller diagrams of T_b along the 6 m-isobath (Fig. 6d) and 15 m-isobath (Fig. 6e) around Gotland in August 2023. The first is the approximate depth of the desalination intake pipes, while the latter targets displacements of summer Baltic Sea thermocline (sect. 1.4).

At the 6 m-isobath (Fig. 6d), the occurrence of water below 12° C is evident only on the southeast coast of Gotland (100 km from the southern tip and including HER) and occurs in two pulses related to upwelling events: a weaker one during the 5-6th of August (seen only at the southern tip of Gotland), and another one during Hans starting simultaneously on 11 August over the entire south-east sector. Hans' upwelling signature lasts only a couple of days on the eastern coast where HER is located (see time series at the points A-D in Figure 5b), and about a week at the southern tip (see time series at the shallowest points A-D in Figure 5b). There is no clear signal propagation at this depth at the south-southeast sector. There is a hint for a signal propagation during Hans at KVA, but the T_b variations are very weak here so it is inconclusive.

https://doi.org/10.5194/egusphere-2026-1344
Preprint. Discussion started: 27 March 2026

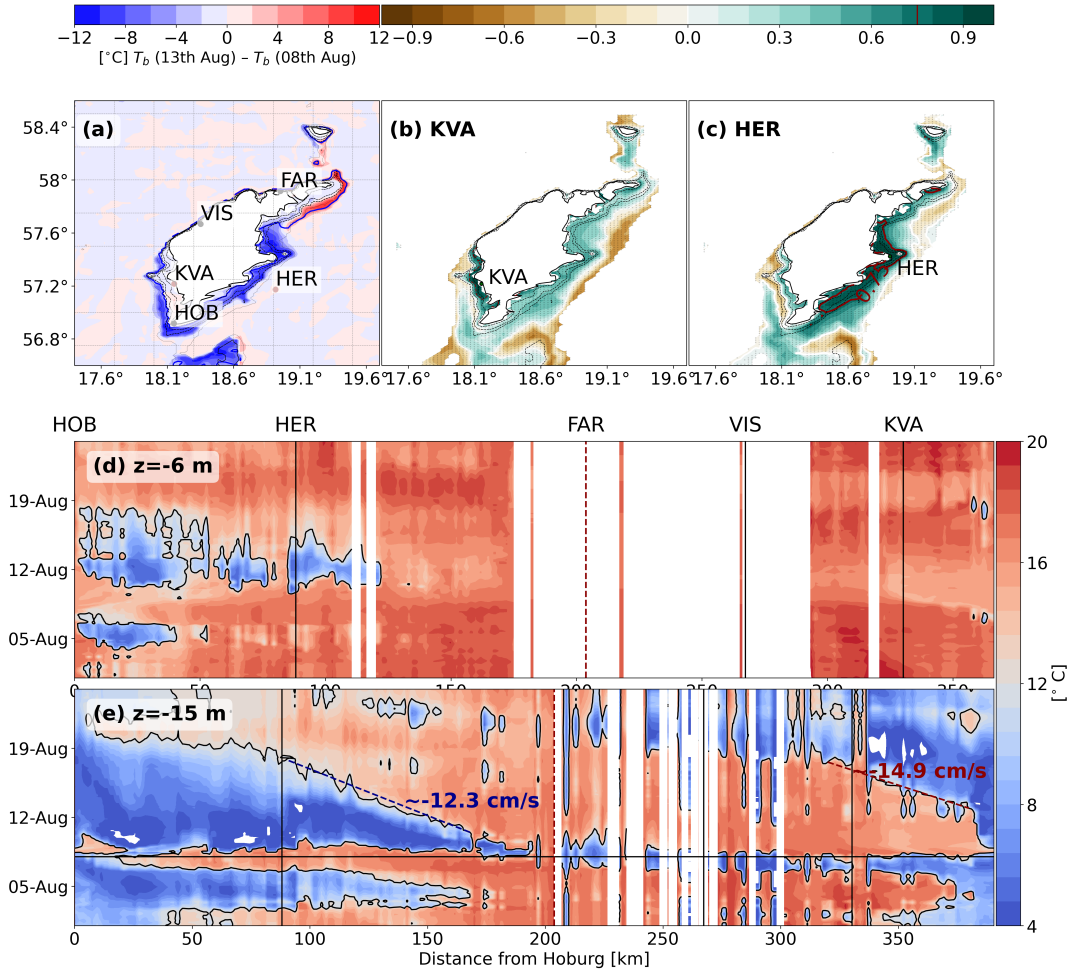

Figure 6. Top left: The difference in ocean model bottom temperature Tb between the 13th August and the 8th August. The solid blue line marks the 12°C-isotherm during the 13th of August, and the dashed black line marks the 20 m-isobath. Red markers indicate the locations of desalination plants at Kvarnåkershamn (KVA) and Herrvik (HER). Black markers denote the positions of Farösund (FAR), Hoburg (HOB), Visby (VIS), and Österngarnsholm (OST) as reference points for Hovmöller diagrams (below). **Top right:** Maps of correlation coefficient between T_b time series at the closest grid point to the desalination plant (KVA and HER, respectively, locations marked in green) and every point around Gotland in the area shallower than 60 m in July-August 2023. Solid red line represents correlation value of 0.75. The white dashed line marks noll correlation. The points with insignificant correlation are not shown. Solid black line represents the 20 m-isobath. **Middle-Bottom** (d-e) Hovmöller diagrams of temperature at 6 m- (d) and at 15 m-isobath (e). The positive x-axis represent the distance from the southern tip (Hoburg, HOB, $x = 0$) following counterclockwise the isobath contour. Vertical solid black lines represent the location of the two desalination plants (HER and KVA), marked is also the Visby (VIS), Farösund (FAR) and Hoburg (HOB). Black dashed lines in (c) are used to estimate speed of the propagating signal. The speed on the eastern coast (= 12.3 cm/s) has been estimated over the [98-160] km, while the one on the western coast (= 14.9 cm/s) over [380-320] km distance.

https://doi.org/10.5194/egusphere-2026-1344
Preprint. Discussion started: 27 March 2026

At the 15 m-isobath (Fig. 6e), the cold water signal due to Hans and the preceding upwelling event is much more pronounced over the entire south and south-east sector. The onset of upwelling due to Hans is evident already on the 8th August. The 12°C-isotherm propagates clockwise (with the coast to the right) from the northern tip along the eastern coast to HER (estimated phase propagation speed of 12.3 cm/s, or 10 km/day). Note also that the upwelling signal that is propagated away from the northeast coast southward results in a warm patch at the northeast coast seen in Figure 6a. At the southern tip (HOB), where the bathymetry is more complex, the propagation speed gets harder to estimate. From the southern tip, the upwelling signal propagates clockwise to KVA with a somewhat higher estimated speed of 14.9 cm/s (13 km/day), consistent with a cold water offshore at KVA seen in Figure 6a. The propagation of upwelling signal is also visible at greater depths, and in the salinity. For example, at the 30 m-isobath, the passage of Hans results in saltier bottom waters $\geq$ 7.3 p.s.u (Figure A3).

3.2 Coastal hazard and coastal hazard impact forecast

Since the analyses suggest that coastal hazard variables (cross-shore transport and bottom temperature) respond directly to the wind forcing at HER, and indirectly at KVA, we test if these findings can be used to build linear regression models of these coastal hazards and their negative impacts at the desalination plants. In the following, we will evaluate performance of regression models (equations 4 and 5) and as well as their ability to forecast the negative impacts recorded in the ocean model (Predicted events defined by volume transport exceeding threshold values; see sect. 1.3). Motivated by the delay in the response of the system, and high vector correlation between wind observations and atmospheric forcing of the ocean model (sect. 2.3), we present the wind observations as a predictor and sensitivity studies to selected parameters. The regression models are trained for summer (F2023) and validated in the following summer (F2024).

3.2.1 Zonal velocities and material (volume) transport

The results for the linear regression models of zonal (proxy cross-shore) ocean model transport U at selected model points with wind stress as a predictor (Eq. 4) are presented as Actual-Predicted graphs in Figure 7. The coefficient of determination (fraction explained variance, R^2) for the regression and the percentage of the predicted extreme transport events ($U > 3.5\sigma$) are shown in the lower-right corner of the graphs. The detailed model metrics are shown in Table 1. At the model points A-D located in a shallow coastal area close to KVA (7a-e), the linear regression has R^2= 0.54-0.62 (corresponding to a linear correlation of about 0.75) and the model was able to predict nearly 90%, i.e., all but one of the 11-12 extreme transport events. There is however a pronounced structure in the residuals (the lower transports tend to be underestimated and the extreme ones tend to be overestimated), which suggest to seek more complex models. The performance of the model is worse at point F as well as H-N further away from the coast (Table 1).

https://doi.org/10.5194/egusphere-2026-1344
Preprint. Discussion started: 27 March 2026

At the model points close to HER (7f-j), the number of recorded events in the model grid points varies a lot (2-14) and the linear regression has generally lower performance close to the shore because of the complex cape-like topography making the ocean currents to veer. The best performance is shown by points B and I south of HER (Fig. 7g-h), with R^2 = 0.3 (0.4) and 100% (50%) predicted events at B (I).

The validation of the linear regression model in the following summer (F2024) is shown in Table 1. We got no impact reports from desalination plants for summer 2024 due to unremarkable summer conditions.There were no extreme transport events at KVA and only a couple of events at HER which were not predicted.

Different projections of wind stress or ocean velocity and introducing a delay of about the inertial period for transport does not change significantly the linear regression results (sensitivity to the projections are presented in figure A4).

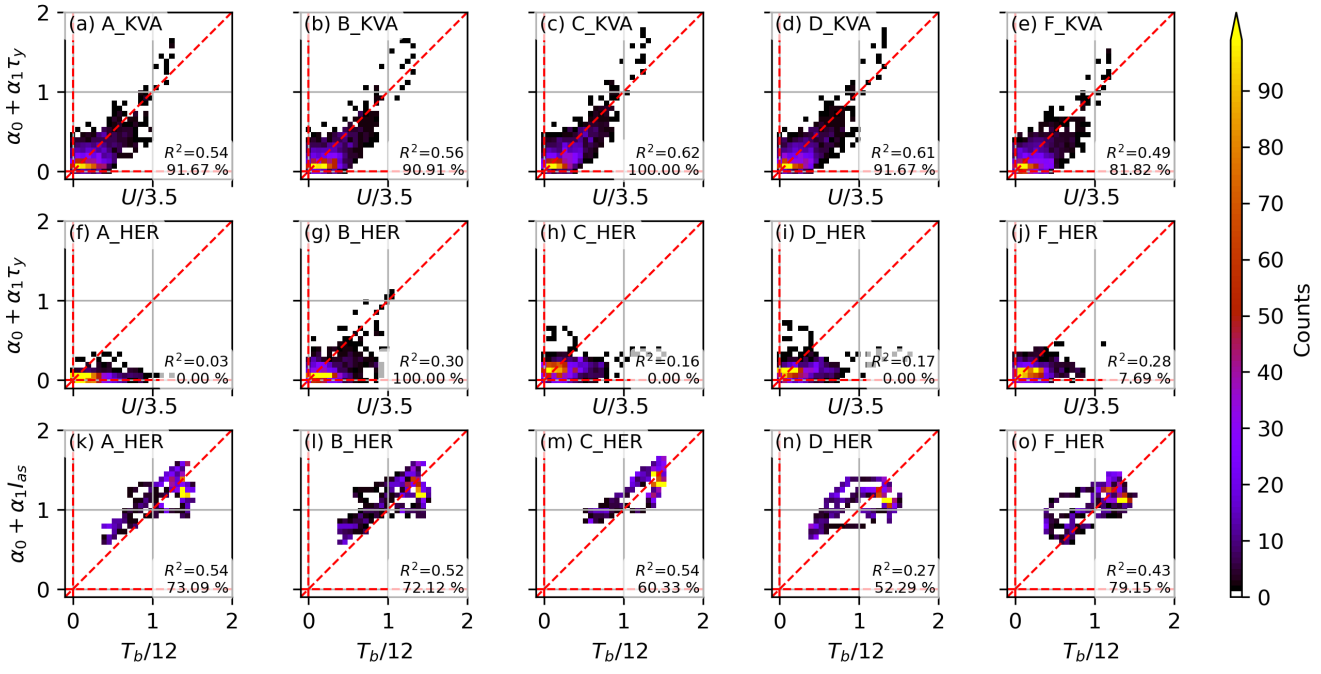

Figure 7. Actual-Predicted histograms for the linear regression of zonal (proxy-cross-shore) transport (U) and extreme transport events ($U > 3.5\sigma$) at KVA (top row, a-e) and HER (f-j) as well as for the bottom temperature and cold spell ($T_b/12 < 1$, k-o). In every scatterplot, the histogram is shown for a different grid point, see Figure 5 for the location. There were 1464 hourly time points in the time series. The coefficient of determination R^2 and the number of predicted negative hazards events are reported in the lower right corner. See text and Tables 1-2 for more information.

https://doi.org/10.5194/egusphere-2026-1344
Preprint. Discussion started: 27 March 2026

Table 1: Performance metrics for linear regression models of the zonal (proxy cross-shore) transport ($U/(3.5\sigma)$) evaluated at ocean model grid points around KVA and HER in summer 2023. Position of the points are marked in Fig. 3. The linear regression model is trained for the ocean model output in summer 2023 (In-sample F2023) using the wind stress at HOB as a predictor (Eq.4). The validation of the regression model is done using ocean model output in the subsequent summer (F2024). The metrics include the number of identified extreme transport events ($|U| > 3.5\sigma$, see below) in a given model point, percentage of correctly predicted events (relative to the total number of events), the coefficient of determination (R^2), the non-dimensional root-mean-square error (RMSE) and the standard deviation σ [m s^{-1}]. The regression results are statistically significant at 95% confidence level ($p < 0.05$).

KVA – In-sample (F2023)							
Station	A	B	C	D	F	H	N
Events (count)	12	11	11	12	11	12	11
Predicted (%)	91.7	90.9	100.0	91.7	81.8	83.3	72.7
R^2	0.54	0.56	0.62	0.61	0.49	0.54	0.43
RMSE	0.20	0.19	0.18	0.18	0.21	0.19	0.22
σ [m s^{-1}]	0.036	0.038	0.063	0.047	0.041	0.038	0.039
KVA – Validation (F2024)							
Events (count)	0	0	0	0	0	0	0
Predicted (%)	-	-	-	-	-	-	-
R^2	0.43	0.49	0.56	0.53	0.36	0.40	0.27
RMSE	0.23	0.20	0.19	0.20	0.23	0.22	0.245
σ [m s^{-1}]	0.032	0.035	0.057	0.040	0.038	0.033	0.037
HER – In-sample (F2023)							
Station	A	B	C	D	F	I	P
Events (count)	5	2	10	11	13	14	9
Predicted (%)	0.0	100.0	0.0	0.0	7.7	50.0	44.4
R^2	0.03	0.30	0.16	0.17	0.28	0.46	0.370
RMSE	0.28	0.24	0.26	0.26	0.24	0.21	0.227
σ [m s^{-1}]	0.013	0.019	0.031	0.015	0.024	0.042	0.036
HER – Validation (F2024)							
Events (count)	2	5	0	0	3	3	3
Predicted (%)	0	0	-	-	0	0	0
R^2	0.005	0.21	0.07	0.06	0.15	0.34	0.222
RMSE	0.29	0.25	0.28	0.28	0.26	0.23	0.252
σ [m s^{-1}]	0.013	0.017	0.031	0.015	0.021	0.038	0.033

https://doi.org/10.5194/egusphere-2026-1344
Preprint. Discussion started: 27 March 2026

Table 2: Performance metrics for models of the bottom temperature ($T_b/12^oC$) evaluated at ocean model grid points around KVA and HER in summer 2023. Position of the points are marked in Fig. 5. The top block shows the linear correlation between the ocean model (F2023) output in the grid points and temperature measurements at the KVA water intake station. The remaining blocks show results from the linear regression model for the bottom temperature around KVA and HER trained for the ocean model output in summer 2023 (In-sample F2023) using the wind impulse as a predictor (Eq.5). The validation of the regression model is done using ocean model output in the subsequent summer (F2024). The metrics include the number of identified cold spells (count) in a given model point, percentage of correctly predicted events (relative to the total number of cold spells), the coefficient of determination (R^2), and the non-dimensional root-mean-square error (RMSE). The correlation and regression are statistically significant at 95% confidence level ($p < 0.05$).

Correlation with observations at KVA water intake							
F2023	A	B	C	D	F	H	N
	0.48	**0.46**	**0.21**	**0.45**	**0.70**	**0.69**	**0.50**
KVA — In-sample (F2023)							
Cold spells (count)	0	0	0	0	109	112	801
Predicted (%)	-	-	-	-	0	0	92.6
R^2	0.18	0.32	0.47	0.17	0.08	0.11	0.47
RMSE	0.10	0.08	0.08	0.10	0.22	0.22	0.25
KVA — Validation (F2023)							
Cold spells (count)	0	0	0	0	80	81	818
Predicted (%)	-	-	-	-	0	0	91
R^2	-0.11	-0.29	-0.10	-0.13	0.15	0.16	-0.12
RMSE	0.12	0.11	0.11	0.10	0.19	0.18	0.35
HER — In-sample (F2023)							
Station	A	B	C	D	F	I	P
Cold spells (count)	275	312	184	459	355	355	506
Predicted (%)	73	72	60	52	80	76	70
R^2	0.54	0.52	0.54	0.27	0.43	0.46	0.45
RMSE	0.20	0.21	0.12	0.28	0.22	0.22	0.24
HER — Validation (F2024)							
Cold spells (count)	114	123	64	159	195	158	364
Predicted (%)	74	65	0	71	59	70	57
R^2	0.23	0.23	0.27	-0.25	0.35	0.35	0.43
RMSE	0.20	0.20	0.17	0.28	0.21	0.20	0.23

https://doi.org/10.5194/egusphere-2026-1344
Preprint. Discussion started: 27 March 2026

3.2.2 Bottom temperature and cold water spells

The results for the linear regression models of bottom temperature T_b at selected model points with wind impulse as a predictor (Eq. 5) are presented in Table 2 and for HER in the bottom row of Figure 7(k-o).

In KVA, no cold spells events occur during the Poly and Hans storms, but some events are registered in the observations at the intake station as well as at the grid points (F,H and N) during a NW wind event (upwelling favorable on the western Gotland coast) on the 17-21 of August (see time series in figure 5b). Linear regression on observations from intake station yields small determination coefficient (R^2=0.05). For the model grid points C and N, R^2=0.47 and lower for the other points.

At HER, the performance of the linear regression models is higher reflecting the coastal upwelling response (sect. 3.1.3) with R^2 of about 0.5 and over 70-80% predicted events at points A-B and F-P (south and offshore off HER). Points C-D located north of the HER have lower performance due to the turning of the coastal jet at the cape causing a delayed response (sect. 3.1.2-3.1.3, Fig. 5b). For the validation period in 2024, the number of cold spells is reduced by 60% and we note a reduction in R^2 but the fraction of predicted cold spells as about the same as in 2023.

4 Discussion

4.1 Summary and discussion of the results

Summer 2023 witnessed two intense wind storms in the Baltic Sea region: Poly and Hans, both associated with SW winds. The Hans storm featured stronger wind velocities than Poly (equal to and exceeding 98th percentile in the observed hourly averages since 2010) and caused disturbance in the operation of the desalination plants on Gotland (Kvarnåkershamn, KVA, southwest coast and Herrvik, HER, southeast coast, figure 1). We built upon the reports of negative coastal hazard impacts of Hans at the desalination plants and analyzed the sparse observations (temperature and salinity at the KVA intake station) and available state-of-the-art operational model output in view of developing an observational, analysis and forecast framework to secure future water resources on Gotland.

We identified three major coastal hazards and their impacts on the desalination plants: [1] extreme ocean velocities and material transport clogging the filters and requiring manual maintenance; [2] cold water spells during summer prompting the change to winter operation mode, and [3] high turbidity decreasing water quality and desalination efficiency. In this study we focus on [1] and [2]. We established that zonal (proxy cross-shore) ocean transport serves to monitor hazard [1] (hazard impact for $U > 3.5\sigma$) and bottom sea temperature serves to monitor hazard [2] (hazard

https://doi.org/10.5194/egusphere-2026-1344
Preprint. Discussion started: 27 March 2026

impact for $T_b < 12°C$).

We analyzed the ocean model response to Hans on a basin-scale and in the closest model grid points in order to identify the coastal hazard drivers (sect. 1.4) that led to negative coastal hazard impacts of Hans. The dominant response on the southeast Gotland coast close to the HER was found to be a coastal upwelling jet (Csanady, 1982b), associated with surface Ekman transport, leading to drop in the bottom temperature due to compensating transport confined in the bottom boundary layer (Lehmann and Myrberg, 2008; Masini et al., 2025). However, the jet tends to turn north and recirculate at the cape-like topography close to HER causing high water transport that varied between the near-by model points; the response in model points 2 km southeast of HER is in best agreement with the reported impact. The daily wind variability, interpreted here as sea breeze (Eronn, 2000; Seroka et al., 2018; Dailidė et al., 2022), was found to modulate ocean transport response close to the coast. The vertical mixing (as represented in the ocean model) was not pronounced at HER.

The ocean response at KVA was found to be more complex. It was not the direct linear coastal response to the SW winds (downwelling jet) that was in action here, but instead, an indirect response to the extreme upwelling at the Swedish coast leading to the increased southward export out of the Western Gotland Basin (between Öland and Gotland). Because of the shoaling close to the KVA, the southward export turns cyclonically due to conservation of potential vorticity. This leads to a recirculation and strong northwest flow at KVA. The shallow coastal bay-like area close to KVA is also subject to ocean transport modulation due to sea breeze. The bottom temperature shows weaker variability in general, and linear coastal response to wind is only evident later during August during NW winds (upwelling favorable at KVA). The ocean model temperature appeared however affected by wind-induced mixing during Hans homogenizing the water column. The bottom temperature in the model grid points a few kilometers further offshore showed a good agreement with the temperature measured at the intake station at KVA.

We found no clear evidence of the CTWs in the shallow grid points at HER and KVA. We found however the hints of CTWs further from the coast where EOF-1 of the meridional (proxy along-shore) velocity was trapped at the slope at about 20 m depth at HER. Also bottom temperature and salinity showed a propagation along 15 m- and 30 m- isobath with the coast to the right. The propagation speed estimated to be about 15 cm/s northward from the southern tip and about 12 cm/s from the northern tip southward (Fig. 6e), which is 10-15 km/day meaning less than 100 km during the 5-day long wind event. The values estimated here are comparable with estimates from theoretical studies for higher CTWs modes (Fennel et al., 2010). We have attempted to run the model of (Chapman, 1987; Brink, 2006) to analyze the CTW modes, but because of the complex bathymetry, stratification, influence of open-sea and coastal jets, the results were inconclusive, and because of the lack of evidence in relevant implication to the desalination plants, a more detailed study of CTWs around Gotland was deferred to future work.

https://doi.org/10.5194/egusphere-2026-1344
Preprint. Discussion started: 27 March 2026

Given that the analysis showed that the dominant driver of the coastal hazards and hazard impacts at the desalination plants (the zonal transport and connected extreme material transport causing clogging and cold water spells) appeared to be either directly, or indirectly, the linear coastal response to winds, we have tested applicability of linear regression models of coastal hazards and hazard impacts. This was further motivated by the fact that the wind direction in the Baltic Sea is prevailing along-shore regarding the orientation of Gotland (SW winds and NE occurring about 30-40% and 10% of the time, respectively, see e.g., Masini et al. (2025)), and by the fact that SW winds dominated during storms Hans and Poly. We used the ocean model output at the grid points close to the desalination plants as predictand (actual), and as the predictor we used the wind stress (for transport) and wind impulse (for bottom temperature) assuming a linear coastal response to along-shore winds (Csanady, 1982a; Masini et al., 2025). Due to the complexity of the ocean response and other contributing drivers (see above), the fraction of explained variance was not high (0.62 and 0.46 for best performing model points for transport at KVA and HER, respectively, and 0.47 and 0.54 for bottom temperature). Nevertheless, the linear regression models captured 100% of the extreme transport events at least at one near-by model point for both KVA and HER.

Regarding the cold temperature spells during the summer, the regression model could capture 80% of the events close to HER, but did not perform well at KVA because the variability of bottom temperature in the shallow bay-like area was generally low and driven to larger extent by recirculation and other drivers like vertical mixing. However, the ocean model bottom temperature at KVA compares favorable with the only available observations (temperature from the intake station) which motivates direct use of operational ocean model output in hazard forecasts for the desalination plants.

4.2 Future outlook

The findings of this study open new possibilities for future hazard impact monitoring and a warning system for the coastal hazards and their impacts on the desalination and drinking water production on Gotland. By analyzing the ocean model output and available observations during the storms Poly and Hans in summer 2023, we established that the ocean model transport and bottom temperature can serve as monitoring variables for 1) extreme material transport and clogging associated with storms, and 2) cold temperature spells associated with upwelling. Moreover, the ocean model bottom temperature compares favorable with the only available observations (temperature from the intake station of KVA). This motivates the use of the ocean model output at the selected grid points close to the desalination plants (as guided by this study) and the threshold values to produce forecasts for the desalination plants, in addition to the statistical models.

https://doi.org/10.5194/egusphere-2026-1344
Preprint. Discussion started: 27 March 2026

We have identified the contributing drivers of the coastal hazards and concluded that the dominating response at HER is the linear coastal upwelling response to winds and it can be captured by linear regression with the wind stress (for extreme transport and clogging) and the wind impulse (for bottom temperature and cold spells) as predictors. At KVA, the coastal upwelling response acts indirectly, and linear regression model performs only for the extreme transport, not bottom temperature. The linear regression models can be developed and tuned further. For example, we have used the zonal velocity as a proxy for cross-shore transport, but tuning the ocean velocity projection at the model grid points in the vicinity of the desalination plants could better capture the coastal current response given the complexity of the local topography.

A higher order model (quadratic, logistic) and weighted regression could be used, and more predictors than just wind stress or wind impulse (also a combination of these two could also be tested), as well as machine-learning models. However, any further tuning and development of the hazard impacts models as well as the validation of the operational model are dependent on the collaboration and continuous validation (through the impact reports) from the desalination plants. It is also necessary to collect hydrographic and current observations in the vicinity of the desalination plants to further validate the operational ocean model and the statistical models.

We focused here on two hazards proxies, extreme transport (for material clogging) and bottom temperature (for cold spells). We do not have any observations of the macro-algae (that are torn from the seabed by wave motions and extreme velocities causing the clogging) or the wave field in the vicinity of the desalination plants. But according to the impact reports, these two contribute to the disturbance only in conjunction with the extreme water velocities, so we assume that they can be "absorbed" in the hazard forecasts of extreme transport events. A future observational and modelling study of the effects of waves is desirable, especially in the shallower coastal area in the vicinity of the desalination plant at Kvarnåkershamn.

We did not address the hazard [3] mentioned in sect. 1.1, namely the turbidity related to, at least partly, the phytoplankton blooms. This is because it was communicated that the impacts due to storms and extreme transport were the priority, and because of the lack of data and adequate model output (turbidity is not included in the output of operational models). Algae sampling around Gotland has been ongoing in the last couple of years under the ALGOTL project and the results are being analyzed and will be presented elsewhere. We have also a dialogue with the desalination plants about the turbidity monitoring in the intake station and data sharing in the future, which will require equipment and personal resources.

https://doi.org/10.5194/egusphere-2026-1344
Preprint. Discussion started: 27 March 2026

5 Conclusions

This study combines analysis of operational model outputs and (sparse) available observations to identify the physical drivers of the coastal hazard impacts on the desalination plants on Gotland associated with the passage of two storms in summer 2023, and to set a framework for forecasting of coastal hazards and their impacts in the future. We focus on two hazards: extreme water transport (impact: clogging the filter membranes), and sudden sea temperature drop during the summer (impact: prompting the change to the winter operation mode).

The southeastern coast of Gotland (where the Herrvik desalination plant is located) exhibits a coastal ocean response to wind forcing aligned with linear theory. The SW winds associated with storm Hans lead to the development of an intense coastal jet and upwelling of cold waters. Linear regression models building upon this finding (with wind stress and wind impulse as predictors) are quite successful in predicting the hazard impacts and pave a way for future development involving more sophisticated forecasts. The southwestern coast of Gotland (hosting the second desalination plant at Kvarnåkershamn) shows a more complex response to SW winds related to a recirculation of the southward current between Öland and Gotland superimposed on inner-shelf variability. A linear regression model captures extreme transport events but not the temperature variability, which is generally low and driven partly by wind driven mixing and other processes. The sea bottom temperature from the operational ocean model agrees well with available observations from the intake station of this desalination plant, suggesting that the model output can be used for user-tailored forecasts.

The future development of coastal hazard impact forecasts to the desalination plants securing the Gotland drinking water resources is contingent on collecting oceanographic observations to validate the operational ocean model and statistical models as well as on a continuous dialogue and reporting from the desalination plants.

6 Acknowledgments

The authors would like to thank Patrik Johansson, Peter Olsson and other members of the Region Gotland's Drinking Water Unit (*Region Gotlands dricksvattenenhet*) as well as Jonas Nilsson for coordination of the Region Gotland's participation in the project. MM would like to thank Johan Nilsson for the valuable discussions. IK and MM would like to thank Lasse Axel for insightful comments regarding operational models. We acknowledge the funding from Formas – a Swedish Research Council for Sustainable Development grant number 2022-02117 ('Ett nytt prognossystem för skadliga algblomningar för tryggare framtida vattenförsörjning och utveckling av turism på Gotland – ALGOTL'). The computations and data analysis were enabled by resources provided by the National Academic Infrastructure for Supercomputing in Sweden (NAISS) at NSC partially funded by the Swedish Research Council through grant agreement no. 2022-06725.

https://doi.org/10.5194/egusphere-2026-1344
Preprint. Discussion started: 27 March 2026

Data availability. The operational model datasets analyzed for this study is publicly available at Copernicus Marine Services (product Baltic Sea Physics Analysis and Forecast at https://data.marine.copernicus.eu/product/BALTICSEA_ANALYSISFORECAST_PHY_003_006/description; historical data older than two years from the current date can be requested with no charge). SMHI wind data are available at https://www.smhi.se/data.

Code and data availability. The Jupyter notebooks and the data to reproduce the manuscript figures using the Copernicus Marine Environment Monitoring Service (CMEMS) products and wind observations (SMHI) will be made publicly available at https://git.bolin.su.se/mmasini/mmasini_2025_hans_hazards upon publication of the manuscript.

Author contributions. Conceptualization: IK, MM, LA, BK, AK; data curation: BK; formal analysis: MM, IK; investigation: MM, IK, LA ; methodology: MM, IK; funding acquisition: IK,LA, BK, AK; supervision: IK; Writing (original draft preparation): MM, IK; Writing (review and editing): MM, IK, AK, BK, LA

Competing interests. The authors declare that they have no conflict of interest.

https://doi.org/10.5194/egusphere-2026-1344
Preprint. Discussion started: 27 March 2026

7 Appendix figures

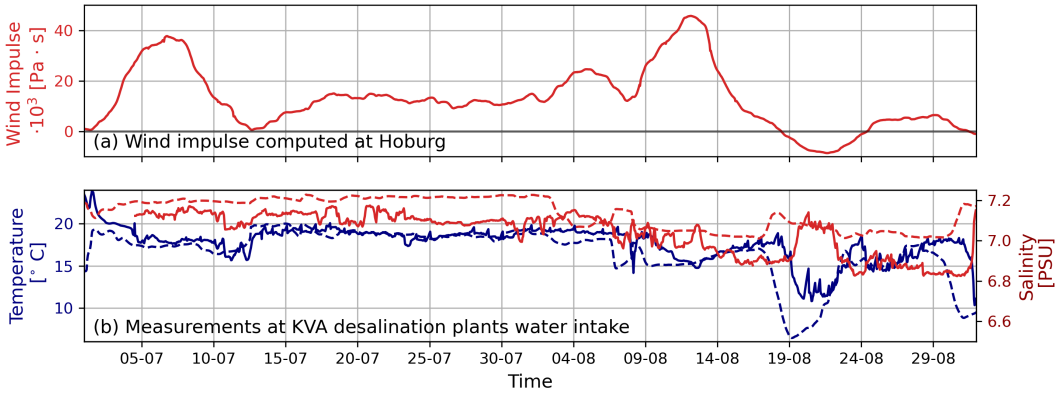

Figure A1. a) Wind impulse computed using Equation 6 and data from Hoburg meteorological station. (b) Solid lines: Timeseries of Temperature (ITS-90, [° C]) and Practical Salinity [p.s.u.] measured at the intake station of the desalination plant in Kvarnåkershamn (KVA) between 29 June and 13 September 2023. Dashed lines: Timeseries of bottom temperature and salinity from the closest operational model grid point F which shows the highest correlation with observation ($r = 0.70$, Table 2), the location is marked in Figure 5c.

https://doi.org/10.5194/egusphere-2026-1344
Preprint. Discussion started: 27 March 2026

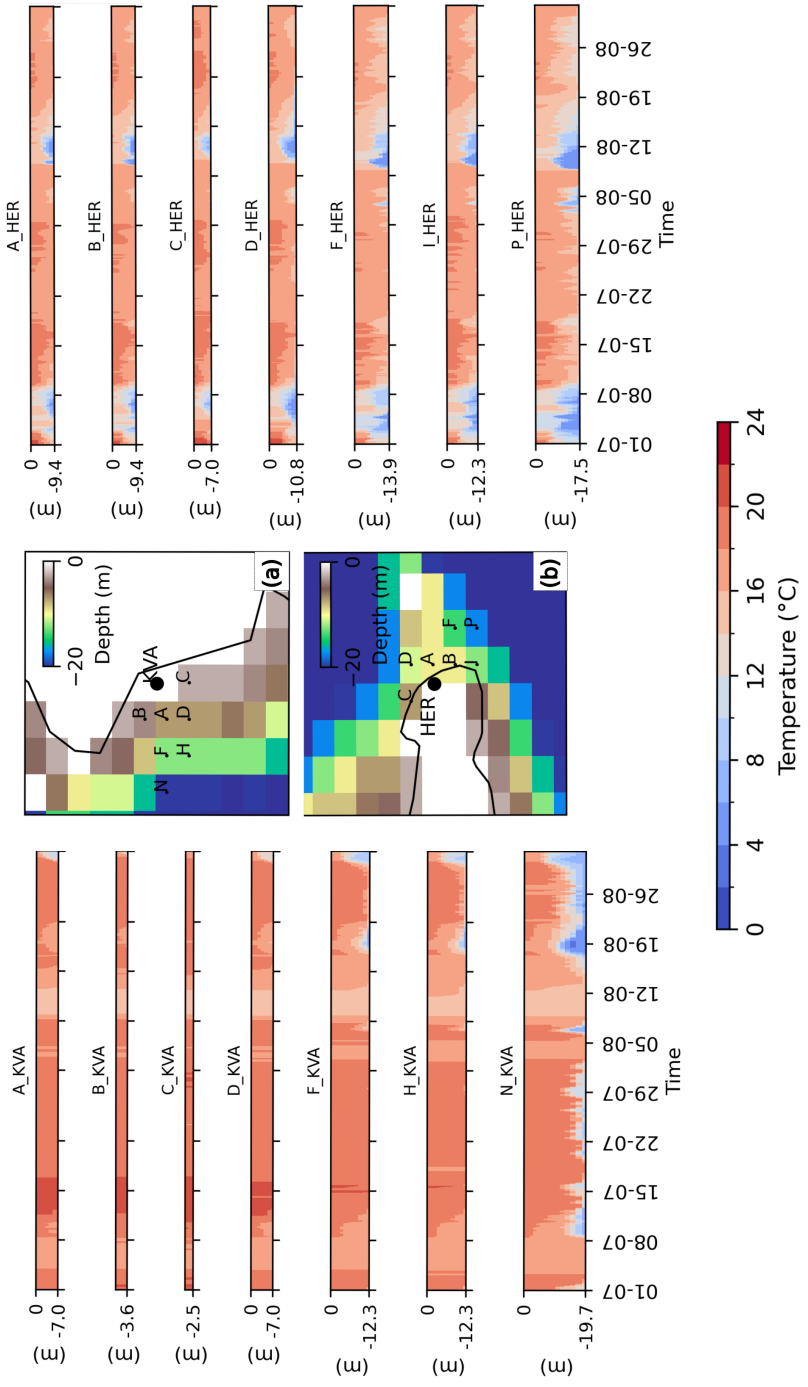

Figure A2. Hovmöller diagrams of temperature [° C] at the ocean model grid points in the vicinity of Herrvik (left) and Kvarnåkershamn (right) in the period of 1-25 August 2023. Location of the points is shown in panels (a) and (b) with color indicating sea bottom depth.

https://doi.org/10.5194/egusphere-2026-1344
Preprint. Discussion started: 27 March 2026

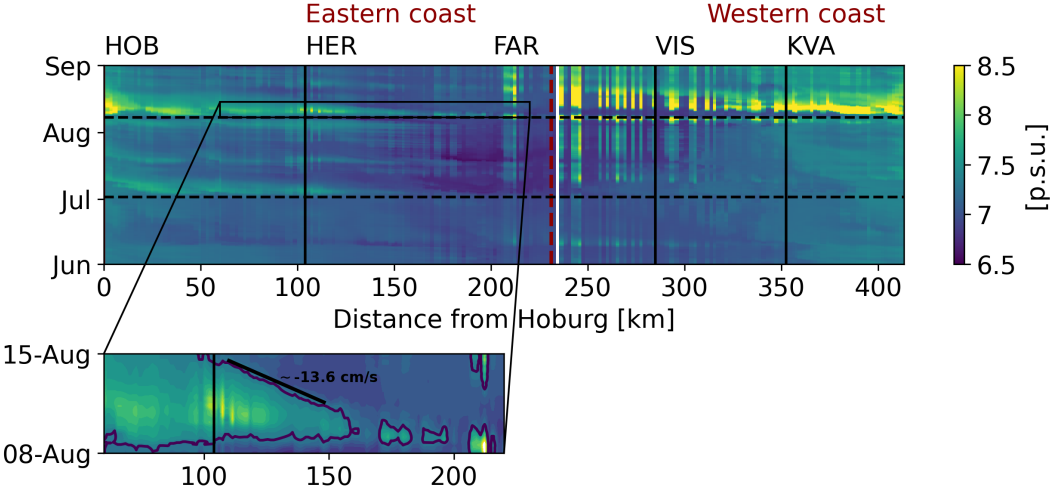

Figure A3. Hovmöller diagrams of salinity at the 30 m-isobath around Gotland. The positive x-axis represents the distance from the southern tip of Gotland (Hoburg, $x = 0$), following the 30 m isobath counter-clockwise. Vertical solid black lines indicate the locations of the desalination plants at Herrvik (HER) and Kvarnåkershamn (KVA), as well as Visby (VIS), Fårösund (FAR), and Hoburg (HOB). Horizontal black dashed lines highlight the onset of Poly (2 July 2023) and Hans (8 August 2023) storms.

https://doi.org/10.5194/egusphere-2026-1344
Preprint. Discussion started: 27 March 2026

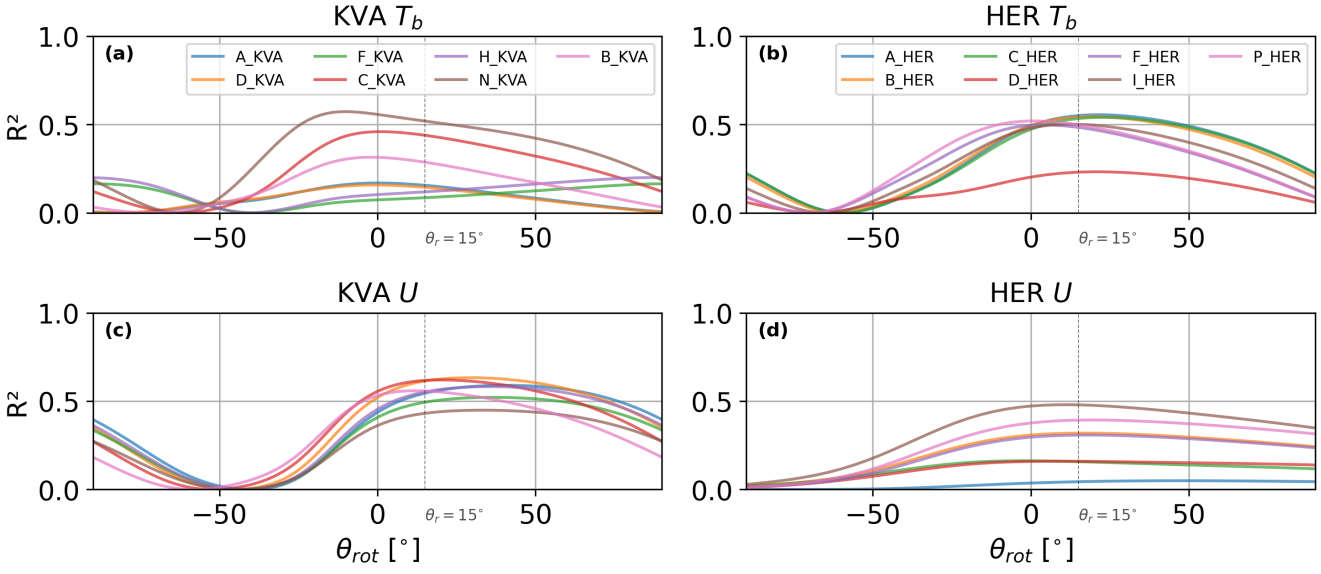

Figure A4. Sensitivity of the determination coefficient R^2 of the linear regression models to the rotation angle of the wind at Hoburg (HOB) for the ensemble of grid points at Kvarnåkerhamn (KVA in a-c, left column) and Herrvik (HER in b-d, right column). The upper row (panels a-b): sensitivity of the linear regression model for T_b using the wind impulse (eq. 5). Bottom row (panels c-d): sensitivity of the linear regression model for the zonal transport U using the wind (eq. 4). The angle of 15° for which the results are presented in sect. 3.2 is indicated by the vertical dashed line.

https://doi.org/10.5194/egusphere-2026-1344
Preprint. Discussion started: 27 March 2026

References

Anderson, D. M., Boerlage, S. F. E., and B, D. M.: Harmful Algal Blooms (HABs) and Desalination: A Guide to Impacts, Monitoring and Management, Intergovernmental Oceanographic Commission, 2017.

Austin, J. A. and Lentz, S. J.: The Inner Shelf Response to Wind-Driven Upwelling and Downwelling, Journal of Physical Oceanography, 32, 2171–2193, https://doi.org/10.1175/1520-0485(2002)032<2171:TISRTW>2.0.CO;2, 2002.

Bauer, P., Beljaars, A., Ahlgrimm, M., Bechtold, P., Bidlot, J., Bonavita, M., Bozzo, A., Forbes, R., Hólm, E., Leutbecher, M., Lopez, P., Magnusson, L., Prates, F., Rodwell, M., Sandu, I., Untch, A., and Vitart, F.: Model Cycle 38r2: Components and Performance, Tech. Rep. Technical Memorandum No. 704, European Centre for Medium-Range Weather Forecasts (ECMWF), https://doi.org/10.21957/xc1r0lj6l, 2013.

Brink, K. H.: Coastal-trapped waves with finite bottom friction, Dynamics of Atmospheres and Oceans, 41, 172–190, https://doi.org/10.1016/j.dynatmoce.2006.05.001, 2006.

Caron, D. A., Ève Garneau, M., Seubert, E., Howard, M. D., Darjany, L., Schnetzer, A., Cetinić, I., Filteau, G., Lauri, P., Jones, B., and Trussell, S.: Harmful algae and their potential impacts on desalination operations off southern California, Water Research, 44, 385–416, https://doi.org/https://doi.org/10.1016/j.watres.2009.06.051, 2010.

Chapman, D. C.: Application of wind-forced, long, coastal-trapped wave theory along the California coast, Journal of Geophysical Research: Oceans, 92, 1798–1816, https://doi.org/10.1029/JC092iC02p01798, 1987.

Contestabile, P. and Vicinanza, D.: Coastal Vulnerability and Mitigation Strategies: From Monitoring to Applied Research, Water, 12, 2594, https://doi.org/10.3390/w12092594, 2020.

Crosby, D. S., Breaker, L. C., and Gemmill, W. H.: A Proposed Definition for Vector Correlation in Geophysics: Theory and Application, Journal of Atmospheric and Oceanic Technology, 10, 355 – 367, https://doi.org/10.1175/1520-0426(1993)010<0355:APDFVC>2.0.CO;2, 1993.

Csanady, G. T.: Circulation in the Coastal Ocean, Springer Netherlands, Dordrecht, ISBN 978-90-481-8372-2 978-94-017-1041-1, https://doi.org/10.1007/978-94-017-1041-1, 1982a.

Csanady, G. T.: On the Structure of Transient Upwelling Events, Journal of Physical Oceanography, 12, 84–96, https://doi.org/10.1175/1520-0485(1982)012<0084:OTSOTU>2.0.CO;2, 1982b.

Dabuleviciene, T., Vaiciute, D., and Kozlov, I. E.: Chlorophyll-a Variability during Upwelling Events in the South-Eastern Baltic Sea and in the Curonian Lagoon from Satellite Observations, Remote Sensing, 12, 3661, https://doi.org/10.3390/rs12213661, 2020.

Dailidė, R., Dailidė, G., Razbadauskaitė-Venskė, I., Povilanskas, R., and Dailidienė, I.: Sea-Breeze Front Research Based on Remote Sensing Methods in Coastal Baltic Sea Climate: Case of Lithuania, Journal of Marine Science and Engineering, 10, https://doi.org/10.3390/jmse10111779, 2022.

Eronn, I.: Effects of a Sea Breeze Circulation on Fluxes in the Marine Boundary Layer Over the Baltic Sea, Uppsala University, ISBN 0511010184 virtual (netLibrary Edition), https://doi.org/DiVA.org:uu-392488, 2000.

Fennel, W. and Seifert, T.: Kelvin wave controlled upwelling in the western Baltic, Journal of Marine Systems, 6, 289–300, https://doi.org/10.1016/0924-7963(94)00038-D, 1995.

Fennel, W., Radtke, H., Schmidt, M., and Neumann, T.: Transient upwelling in the central Baltic Sea, Continental Shelf Research, 30, 2015–2026, https://doi.org/10.1016/j.csr.2010.10.002, 2010.

https://doi.org/10.5194/egusphere-2026-1344
Preprint. Discussion started: 27 March 2026

Hajdu, S., Höglander, H., and Larsson, U.: Phytoplankton vertical distributions and composition in Baltic Sea cyanobacterial blooms, Harmful Algae, 6, 189–205, https://doi.org/https://doi.org/10.1016/j.hal.2006.07.006, 2007.

Johansson, H.: Strategic Assessment of Sweden's Water Future., Tech. rep., Chalmers University of Technology, 2020.

Kahru, M., Savchuk, O. P., and Elmgren, R.: Satellite measurements of cyanobacterial bloom frequency in the Baltic Sea: interannual and spatial variability, Marine Ecology Progress Series, 343, 15–23, https://doi.org/10.3354/meps06943, 2007.

Karlson, B., Andersen, P., Arneborg, L., Cembella, A., Eikrem, W., John, U., West, J. J., Klemm, K., Kobos, J., Lehtinen, S., Lundholm, N., Mazur-Marzec, H., Naustvoll, L., Poelman, M., Provoost, P., De Rijcke, M., and Suikkanen, S.: Harmful algal blooms and their effects in coastal seas of Northern Europe, Harmful Algae, 102, 101 989, https://doi.org/https://doi.org/10.1016/j.hal.2021.101989, global Harmful Algal Bloom Status Reporting, 2021.

Kärnä, T., Ljungemyr, P., Falahat, S., Ringgaard, I., Axell, L., Korabel, V., Murawski, J., Maljutenko, I., Lindenthal, A., Jandt-Scheelke, S., Verjovkina, S., Lorkowski, I., Lagemaa, P., She, J., Tuomi, L., Nord, A., and Huess, V.: Nemo-Nordic 2.0: operational marine forecast model for the Baltic Sea, Geoscientific Model Development, 14, 5731–5749, https://doi.org/10.5194/gmd-14-5731-2021, 2021.

Koszalka, I., LaCasce, J. H., and Orvik, K. A.: Relative dispersion in the Nordic Seas, Journal of Marine Research, 67, 411–433, https://doi.org/10.1357/002224009790741102, 2009.

Kullenberg, G.: Chapter 3 Physical Oceanography, in: Elsevier Oceanography Series, edited by Voipio, A., vol. 30 of *The Baltic Sea*, pp. 135–181, Elsevier, https://doi.org/10.1016/S0422-9894(08)70140-5, 1981.

Lass, H.-U., Mohrholz, V., Nausch, G., and Siegel, H.: On phosphate pumping into the surface layer of the eastern Gotland Basin by upwelling, Journal of Marine Systems, 80, 71–89, https://doi.org/10.1016/j.jmarsys.2009.10.002, 2010.

Ledesma, M., Gorokhova, E., Garbaras, A., Röjning, L., Brena, B., and Karlson, A. M. L.: High capacity for a dietary specialist consumer population to cope with increasing cyanobacterial blooms, Sci. Rep., 12, 22 169, https://doi.org/https://doi.org/10.1038/s41598-022-26611-2, 2022.

Lehmann, A. and Myrberg, K.: Upwelling in the Baltic Sea — A review, Journal of Marine Systems, 74, S3–S12, https://doi.org/https://doi.org/10.1016/j.jmarsys.2008.02.010, 2008.

Lehmann, A., Myrberg, K., and Höflich, K.: A statistical approach to coastal upwelling in the Baltic Sea based on the analysis of satellite data for 1990–2009, Oceanologia, 54, 369–393, 2012.

Lentz, S. J. and Chapman, D. C.: The Importance of Nonlinear Cross-Shelf Momentum Flux during Wind-Driven Coastal Upwelling, Journal of Physical Oceanography, 34, 2444–2457, https://doi.org/10.1175/JPO2644.1, 2004.

Leppäranta, M. and Myrberg, K.: Physical Oceanography of the Baltic Sea, Springer, Berlin, Heidelberg, ISBN 978-3-540-79702-9 978-3-540-79703-6, https://doi.org/10.1007/978-3-540-79703-6, 2009.

Lips, I. and Lips, U.: Abiotic factors influencing cyanobacterial bloom development in the Gulf of Finland (Baltic Sea), Hydrobiologia, 614, 133–140, https://doi.org/10.1007/s10750-008-9449-2, 2008.

Martín Míguez, B., Heslop, E., Bax, N., Benedetti-Cecchi, L., Canonico, G., Currie, K., Evans, K., Fischer, A. S., Garçon, V., Hood, M., Karstensen, J., Lara-López, A., Legler, D., Muller-Karger, F. E., Nair Thayannur Mullachery, B., Nordlund, L. M., Palacz, A. P., Post, J., Simmons, S. E., Speich, S., Stukonytė, L., Sutton, A. J., Tanhua, T., Telszewski, M., von Schuckmann, K., Waite, A. M., and Yu, W.: GOOS Essential Ocean Variables: the backbone of a sustained and evolving global ocean observing system, Frontiers in Marine Science, Volume 13 - 2026, https://doi.org/10.3389/fmars.2026.1737002, 2026.

https://doi.org/10.5194/egusphere-2026-1344
Preprint. Discussion started: 27 March 2026

Masini, M., Koszalka, I., Nilsson, J., Sokolov, A., and Gustafsson, B.: Dynamics of Upwelling and Downwelling in a Channel Basin of the Baltic Sea, Tellus A: Dynamic Meteorology and Oceanography, 77, 38–66, https://doi.org/https://doi.org/10.16993/tellusa.4070, 2025.

Meier, H. E. M., Rutgersson, A., and Reckermann, M.: An Earth System Science Program for the Baltic Sea Region, Eos, Transactions American Geophysical Union, 95, 109–110, https://doi.org/10.1002/2014EO130001, _eprint: https://agupubs.onlinelibrary.wiley.com/doi/pdf/10.1002/2014EO130001, 2014.

Meier, H. E. M., Kniebusch, M., Dieterich, C., Gröger, M., Zorita, E., Elmgren, R., Myrberg, K., Ahola, M. P., Bartosova, A., Bonsdorff, E., Börgel, F., Capell, R., Carlén, I., Carlund, T., Carstensen, J., Christensen, O. B., Dierschke, V., Frauen, C., Frederiksen, M., Gaget, E., Galatius, A., Haapala, J. J., Halkka, A., Hugelius, G., Hünicke, B., Jaagus, J., Jüssi, M., Käyhkö, J., Kirchner, N., Kjellström, E., Kulinski, K., Lehmann, A., Lindström, G., May, W., Miller, P. A., Mohrholz, V., Müller-Karulis, B., Pavón-Jordán, D., Quante, M., Reckermann, M., Rutgersson, A., Savchuk, O. P., Stendel, M., Tuomi, L., Viitasalo, M., Weisse, R., and Zhang, W.: Climate change in the Baltic Sea region: a summary, Earth System Dynamics, 13, 457–593, https://doi.org/10.5194/esd-13-457-2022, 2022.

Merz, B., Kuhlicke, C., Kunz, M., Pittore, M., Babeyko, A., Bresch, D. N., Domeisen, D. I. V., Feser, F., Koszalka, I., Kreibich, H., Pantillon, F., Parolai, S., Pinto, J. G., Punge, H. J., Rivalta, E., Schröter, K., Strehlow, K., Weisse, R., and Wurpts, A.: Impact Forecasting to Support Emergency Management of Natural Hazards, Reviews of Geophysics, 58, e2020RG000704, https://doi.org/https://doi.org/10.1029/2020RG000704, 2020.

Müller, M., Homleid, M., Ivarsson, K.-I., Køltzow, M. A. Ø., Lindskog, M., Midtbø, K. H., Andrae, U., Aspelien, T., Berggren, L., Bjørge, D., Dahlgren, P., Kristiansen, J., Randriamampianina, R., Ridal, M., and Vignes, O.: AROME-MetCoOp: A Nordic Convective-Scale Operational Weather Prediction Model, Weather and Forecasting, 32, 609–627, https://doi.org/10.1175/WAF-D-16-0099.1, 2017.

Neumann, T., Radtke, H., Cahill, B., Schmidt, M., and Rehder, G.: Non-Redfieldian carbon model for the Baltic Sea (ERGOM version 1.2) – implementation and budget estimates, Geoscientific Model Development, 15, 8473–8540, https://doi.org/10.5194/gmd-15-8473-2022, 2022.

Persson, A.: The Story of the Hovmöller Diagram: An (Almost) Eyewitness Account, Bulletin of the American Meteorological Society, 98, 949 – 957, https://doi.org/10.1175/BAMS-D-15-00234.1, 2017.

Pizarro, O. and Shaffer, G.: Wind-Driven, Coastal-Trapped Waves off the Island of Gotland, Baltic Sea, Journal of Physical Oceanography, 28, 2117–2129, https://doi.org/10.1175/1520-0485(1998)028<2117:WDCTWO>2.0.CO;2, 1998.

Roy, A. G., Biron, P. M., and Lapointe, M. F.: Implications of low-pass filtering on power spectra and autocorrelation functions of turbulent velocity signals, Math. Geol, 29, 653–668, https://doi.org/https://doi.org/10.1007/BF02769649, 1997.

Russo, S., Sillmann, J., and Fischer, E. M.: Top ten European heatwaves since 1950 and their occurrence in the coming decades, Environmental Research Letters, 10, 124003, https://doi.org/10.1088/1748-9326/10/12/124003, 2015.

Rutgersson, A., Kjellström, E., Haapala, J., Stendel, M., Danilovich, I., Drews, M., Jylhä, K., Kujala, P., Larsén, X. G., Halsnæs, K., Lehtonen, I., Luomaranta, A., Nilsson, E., Olsson, T., Särkkä, J., Tuomi, L., and Wasmund, N.: Natural hazards and extreme events in the Baltic Sea region, Earth System Dynamics, 13, 251–301, https://doi.org/10.5194/esd-13-251-2022, 2022.

Salinas-Rodriguez, S. G. and Schippers, J. C.: Seawater Reverse Osmosis Desalination: Assessment and Pre-treatment of Fouling and Scaling, London: IWA Publishing, https://doi.org/10.2166/9781780409863, 2021.

https://doi.org/10.5194/egusphere-2026-1344
Preprint. Discussion started: 27 March 2026

Seroka, G., Fredj, E., Kohut, J., Dunk, R., Miles, T., and Glenn, S.: Sea Breeze Sensitivity to Coastal Upwelling and Synoptic Flow Using Lagrangian Methods, Journal of Geophysical Research: Atmospheres, 123, 9443–9461, https://doi.org/https://doi.org/10.1029/2018JD028940, 2018.

Silva Pinto, F. and Cunha Marques, R.: Desalination projects economic feasibility: A standardization of cost determinants, Renewable and Sustainable Energy Reviews, 78, 904–915, https://doi.org/10.1016/j.rser.2017.05.024, 2017.

Soomere, T. and Keevallik, S.: Anisotropy of moderate and strong winds in the Baltic Proper, Proceedings of the Estonian Academy of Sciences, Engineering, 7, 35–49, 2001.

Vahtmäe, E., Kotta, J., Lõugas, L., and Kutser, T.: Mapping spatial distribution, percent cover and biomass of benthic vegetation in optically complex coastal waters using hyperspectral CASI and multispectral Sentinel-2 sensors, International Journal of Applied Earth Observation and Geoinformation, 102, 102 444, https://doi.org/https://doi.org/10.1016/j.jag.2021.102444, 2021.

Villacorte, L., Tabatabai, S., Dhakal, N., Amy, G., Schippers, J., and Kennedy, M.: Algal blooms: an emerging threat to seawater reverse osmosis desalination, Desalination and Water Treatment, 55, 2601–2611, https://doi.org/https://doi.org/10.1080/19443994.2014.940649, 2015.

Villacorte, L. O., Dixon, M., and E, B. S. F.: Seawater Reverse Osmosis Desalination: Assessment and Pre-treatment of Fouling and Scaling, London: IWA Publishing, https://doi.org/10.2166/9781780409863, 2021.

Von Storch, H. and Zwiers, F. W.: Statistical Analysis in Climate Research, Cambridge University Press, ISBN 0511010184 virtual (netLibrary Edition), https://doi.org/https://doi.org/10.1017/CBO9780511612336, 1999.

Walin, G.: On the hydrographic response to transient meteorological disturbances, Tellus, 24, 169, https://doi.org/10.3402/tellusa.v24i3.10632, 1972a.

Walin, G.: Some observations of temperature fluctuations in the coastal region of the Baltic, Tellus, 24, 187, https://doi.org/10.3402/tellusa.v24i3.10633, number: 3 Publisher: Stockholm University Press, 1972b.

Yang, Z., Zhou, Y., Feng, Z., Rui, X., Zhang, T., and Zhang, Z.: A Review on Reverse Osmosis and Nanofiltration Membranes for Water Purification, Polymers, 11, https://doi.org/10.3390/polym11081252, 2019.

Zhurbas, V., Oh, I. S., and Park, T.: Formation and decay of a longshore baroclinic jet associated with transient coastal upwelling and downwelling: A numerical study with applications to the Baltic Sea, Journal of Geophysical Research: Oceans, 111, https://doi.org/10.1029/2005JC003079, 2006.

Zhurbas, V., Laanemets, J., and Vahtera, E.: Modeling of the mesoscale structure of coupled upwelling/downwelling events and the related input of nutrients to the upper mixed layer in the Gulf of Finland, Baltic Sea, Journal of Geophysical Research: Oceans, 113, https://doi.org/10.1029/2007JC004280, 2008.